HHS Public Access

Author manuscript

Eur J Med Chem. Author manuscript; available in PMC 2018 January 05.

Published in final edited form as:

Eur J Med Chem. 2017 January 05; 125: 515–527. doi:10.1016/j.ejmech.2016.09.053.

Synthesis, evaluation, and CoMFA study of fluoroquinophenoxazine derivatives as bacterial topoisomerase IA inhibitors

Xufen Yu[a,1], **Mingming Zhang**[a,1], **Arasu Annamalai**[b], **Priyanka Bansod**[b], **Gagandeep Narula**[b], **Yuk-Ching Tse-Dinh**[b,c], and **Dianqing Sun**[a,*]

[a]Department of Pharmaceutical Sciences, The Daniel K. Inouye College of Pharmacy, University of Hawai'i at Hilo, 34 Rainbow Drive, Hilo, HI 96720, USA

[b]Department of Chemistry & Biochemistry, Florida International University, Miami, FL 33199, USA

[c]Biomolecular Sciences Institute, Florida International University, Miami, FL 33199, USA

Abstract

New antibacterial agents with novel target and mechanism of action are urgently needed to combat problematic bacterial infections and mounting antibiotic resistances. Topoisomerase IA represents an attractive and underexplored antibacterial target, as such, there is a growing interest in developing selective and potent topoisomerase I inhibitors for antibacterial therapy. Based on our initial biological screening, fluoroquinophenoxazine **1** was discovered as a low micromolar inhibitor against *E. coli* topoisomerase IA. In the literature, fluoroquinophenoxazine analogs have been investigated as antibacterial and anticancer agents, however, their topoisomerase I inhibition was relatively underexplored and there is little structure-activity relationship (SAR) available. The good topoisomerase I inhibitory activity of **1** and the lack of SAR prompted us to design and synthesize a series of fluoroquinophenoxazine analogs to systematically evaluate the SAR and to probe the structural elements of the fluoroquinophenoxazine core toward topoisomerase I enzyme target recognition. In this study, a series of fluoroquinophenoxazine analogs was designed, synthesized, and evaluated as topoisomerase I inhibitors and antibacterial agents. Target-based assays revealed that the fluoroquinophenoxazine derivatives with 9-NH_2 and/or 6-substituted amine functionalities generally exhibited good to excellent inhibitory activities against topoisomerase I with IC_{50}s ranging from 0.24–3.9 μM. Notably, **11a** bearing the 6-methylpiperazinyl and 9-amino motifs was identified as one of the most potent topoisomerase I

*Corresponding author. Dr. Dianqing Sun, Department of Pharmaceutical Sciences, The Daniel K. Inouye College of Pharmacy, University of Hawai'i at Hilo, 34, Rainbow Drive, Hilo, HI 96720, USA., Tel: +1-(808)-933-2960, Fax: +1-(808)-933-2974, dianqing@hawaii.edu (D. Sun).

[1]These two authors contributed equally to this paper.

Conflict of interest

The authors declare no conflict of interest.

Appendix A: Supplementary data

Supplementary data related to this article can be found at

inhibitors (IC_{50} = 0.48 μM), and showed broad spectrum antibacterial activity (MICs = 0.78–7.6 μM) against all the bacteria strains tested. Compound **11g** with the 6-bipiperidinyl lipophilic side chain exhibited the most potent antituberculosis activity (MIC = 2.5 μM, SI = 9.8). In addition, CoMFA analysis was performed to investigate the 3D-QSAR of this class of fluoroquinophenoxazine derivatives. The constructed CoMFA model produced reasonable statistics (q^2 = 0.688 and r^2 = 0.806). The predictive power of the developed model was obtained using a test set of 7 compounds, giving a predictive correlation coefficient r^2_{pred} of 0.767. Collectively, these promising data demonstrated that fluoroquinophenoxazine derivatives have the potential to be developed as a new chemotype of potent topoisomerase IA inhibitors with antibacterial therapeutic potential.

Graphical Abstract

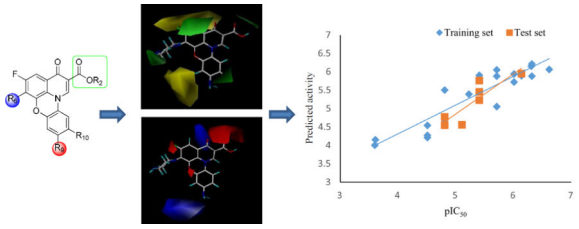

Keywords

Antibacterial; CoMFA analysis; 3D-QSAR; fluoroquinophenoxazine; topoisomerase IA; SAR

1. Introduction

DNA topoisomerases maintain the helical and superhelical structure of DNA and are essential enzymes required for cellular processes and functions including DNA replication, transcription, and repair [1, 2]. Therefore, poison inhibitors of topoisomerase enzymes can lead to the accumulation of the intermediate topoisomerase-DNA cleavage complex and subsequently result in bacterial or cancer cell death [2, 3]. Clinically, topoisomerase enzymes represent attractive and successful targets for anticancer and antibacterial chemotherapy [4, 5]. In contrast, topoisomerase I is underexplored as antibacterial target, thus potent and selective topoisomerase I inhibitors can serve as a promising class of chemotherapeutic agents toward the treatment of problematic bacterial infections [6, 7].

In our ongoing efforts to discover new topoisomerase I inhibitors as antibacterial agents and to probe the topoisomerase I recognition [8, 9], we identified during high-throughput screening (HTS) assay development a compound NSC648059 (**1**, Fig. 1) with low micromolar inhibitory activity (IC_{50} = 0.8–2.0 μM) against *Escherichia coli* topoisomerase I. Structurally, **1** is a fluoroquinophenzoxazine derivative with a unique planar tetracyclic ring system, belonging to a member of an extended chemical class of fluoroquinolone antibiotics. In the clinic, fluoroquinolones including norfloxacin and ciprofloxacin (Fig. 1) represent some of the most successful antibiotic classes, whose mechanisms of action are to inhibit bacterial DNA gyrase and topoisomerase IV as well as relaxation of supercoiled DNA and thus to promote breakage of double-stranded DNA [10]. Specifically,

fluoroquinophenoxazines such as A-62176 and A-85226 (Fig. 1) have been reported as antibacterial [11, 12] and anticancer [13–16] agents. For example, A-62176 exhibited good activity against several cancer cell lines with IC_{50} values ranging from 0.87–4.34 μM [13]. However, their bacterial topoisomerase I inhibition was relatively underexplored and there is little structure-activity relationship (SAR) of fluoroquinophenoxazine derivatives available in the literature [13]. Herein, on the basis of this HTS hit **1**, we describe the design, synthesis, and evaluation of a series of fluoroquinophenoxazine structural analogs, probing their SAR toward bacterial topoisomerase I and other topoisomerases as well as their whole cell antibacterial activity. Additionally, we built and developed a quantitative structure-activity relationship (QSAR) and comparative molecular field analysis (CoMFA) model in an effort to guide further design and synthesis of this class of topoisomerase IA inhibitors.

2. Results and discussion

2.1. Chemistry

To validate the initial assay hit, we first resynthesized 9-amino-5, 6-difluoro-3-oxo-3*H*–pyrido[3,2,1-kl] phenoxazine-2-carboxylic acid (**1**) and retested its biochemical activity against *E. coli* topoisomerase I. Resynthesized fluoroquinophenoxazine hit **1** showed reproducible topoisomerase I inhibitory activity with an IC_{50} of 1.95 μM. The synthesis of **1** is shown in Scheme 1. Briefly, commercially available 2,3-difluoro-6-nitrophenol was hydrogenated using Pd/C (20 mol %) as the catalyst to the corresponding amino product **2**, which can be used in next step without further purification [17]. Subsequent reaction of the aniline derivative **2** with diethyl 2-(ethoxymethylene)malonate under ambient temperature gave **3** in 87% yield. For next nucleophilic displacement cyclization, an improved protocol was developed for this intramolecular cyclization reaction under microwave irradiation at 250 °C instead of conventional heating [11]. Following simple filtration, **4** was obtained in 80% yield. Subsequently, **4** reacted with 1-chloro-2,4-dinitrobenzene (**5a**) in DMF at 100 °C to give the desired tetracyclic product **6a** in 57% yield. Upon treatment of **6a** in acidic condition (AcOH/HCl) under reflux for 4 h, the free carboxylic acid derivative **7a** was obtained by simple filtration in 91% yield. Finally, hydrogenation of **7a** under H_2 (1.0 bar) using $FeSO_4{\cdot}6H_2O$ as the catalyst failed to yield the amine product **1** after 14 h. However, when $SnCl_2$ was used as catalyst and AcOH as the solvent, the nitro group was smoothly reduced into the amino group under reflux for 3 h and the final product **1** was obtained in 86% yield.

Under the optimized conditions, we next expanded the structural diversity of **1** to evaluate the effect of various substituents on the quinophenoxazine skeleton and to explore their SAR. First, we used various substrates **5b–e** in Scheme 2 in an effort to generate a focused set of quinophenoxazine derivatives **7b–e**. It is worthwhile noting that a dramatic difference was observed in terms of the reactivity of the substrate **5** with different electronic and/or physiochemical properties. For example, **5b** bearing an electron-withdrawing nitrile group facilitated the completion of cyclization in 2 h and **6b** was obtained in 59% yield. On the other hand, **5c** with the lipophilic trifluoromethyl group could finish the reaction by extending the reaction time, affording the desired product **6c** in a lower yield (10%). In addition, when the substrate **5d** with an acetyl group was tried, **6d** was obtained in 38%

yield. However, for the substrate with the corresponding fluorine substitution, no reaction occurred even when the reaction temperature was raised to 120 °C. Furthermore, more harsh conditions were tried in an attempt to facilitate the reaction by heating the reaction to 160 °C in a sealed pressure tube or heating the reaction to 200 °C under microwave irradiation, but with not much success. In the case of **5e** with additional nitro and chlorine substituents, the reaction proceeded smoothly and **6e** was obtained in 40% yield. Final ester hydrolysis was performed in acetic acid/hydrochloric acid under reflux, affording free carboxylic acid products **7b–e** in 36–95% yields.

In the course of antibacterial evaluation, we observed compound **1** lost 2–4 fold whole cell antibacterial activity after 4 weeks of storage, indicating that **1** may have stability and/or solubility issue. From our ^{1}H NMR experiments, we also noted that **1** could be easily precipitated out in d_6-DMSO solvent and no degradation-related evidence was observed following several weeks of monitoring **1** in both d_6-DMSO NMR and HPLC experiments (data not shown). Thus, to enhance the overall solubility profile of this class of quinophenoxazine derivatives, we introduced a variety of solubilizing and polar groups into the fluoroquinophenoxazine scaffold by displacing the 6-fluorine atom of **6a, 7a**, or **1** with different amine functionalities such as piperazine, 1-methylpiperazine, and morpholine (Scheme 3) [18]. Specifically, **6a** reacted with 1-methylpiperazine in pyridine at 110 °C to give **9** in 53% yield. Accordingly, **7a** reacted with 1-methylpiperazine and piperazine in pyridine under nitrogen atmosphere at 90 °C, and both reactions proceeded smoothly to afford **10a** and **10b** in 45% and 84% yields, respectively [12]. In the cases of **1** and some other amine substrates, notably, reaction temperature appeared to play a critical role in this nucleophilic displacement reaction. For example, when morpholine was used as a nucleophile, the reaction became complicated under 90 °C, which is suitable for 1-methylpiperazine and piperazine. In contrast, when temperature was reduced to 70 °C, the reaction could be completed in 16 h to produce **11d** in 71% yield. Other functional amines were also subjected to this substitution reaction, and most of the reactions could lead to the desired products **11c–k** under 90 °C in moderate yields except for 1-adamantylamine. We found that the reaction of **1** with 1-adamantylamine could finish under reflux after 4 days in 29% yield, presumably due to steric effect. In addition, to investigate the effect of the free amine functionality of **1** on topoisomerase inhibition and antibacterial activity, we next tried to protect the free amino group with acetyl functionality. The *N*-acetyl derivative **12** was synthesized from **1** and acetic anhydride in pyridine at 80–100 °C and the solid product was collected by simple filtration in high yield (92%).

Finally, to evaluate the potential stereospecific effect at the 6 position of fluoroquinophenoxazine derivatives on biological activity, we designed and synthesized several chiral fluoroquinophenoxazine amine derivatives from **6a** or **1** and chiral amine building blocks [12, 13]. The nucleophilic substitution reaction of **1** and (*S*)-3-(Boc-amino)pyrrolidine (**13a**) in pyridine was completed in 20 h, affording **15a** in 86% yield. Subsequent *N*-Boc deprotection of **15a** produced **17a** in 78% yield upon the treatment with diluted hydrochloric acid. With regard to the reaction of **1** and the corresponding (*R*)-3-(Boc-amino)pyrrolidine (**13b**), the substituted compound **15b** could not be obtained by filtration upon the completion of reaction. Therefore, the crude product **15b** was used for the

following deprotection reaction and the corresponding fluorophenoxazine derivative **17b** (*R*) was obtained in 48% yield over two steps. Accordingly, compound **16** was synthesized from **6a** as the starting material in 32% yield over two steps (Scheme 4).

2.2. Biological testing

All the synthesized target molecules were tested for the ability to inhibit the relaxation activity of *E. coli* topoisomerase I in target-based assay, as well as against a panel of bacterial strains including the wild-type *E. coli* MG1655 K12 strain, *E. coli* strain BAS3023 with *imp* mutation conferring membrane permeability to small molecules [19, 20], the wild-type Gram-positive *B. subtilis* (ATCC 6633) strain, and *M tuberculosis* (H_{37}Rv). The results are summarized in Table 1.

2.2.1. E. coli topoisomerase I inhibition—Biochemical evaluation for inhibition of the relaxation activity of *E. coli* topoisomerase I revealed that the majority of our synthesized compounds possessed good activity against *E. coli* topoisomerase I. On the basis of these topoisomerase I inhibition data (Table 1), an illuminating SAR has been obtained and is summarized in Fig. 2. i). The 9 position substituent plays a very important role in topoisomerase I inhibitory activity. Among the 5,6-difluoroquinophenoxazine derivatives, the hit compound **1** with the electron-donating 9-NH_2 group showed the most potent activity (IC_{50} = 195 μM) against *E. coli* topoisomerase I. Both free carboxylic acid **7c** and its ethyl ester derivative **6c** with the 9-CF_3 functionality were inactive against topoisomerase I when tested at 125 μM. In addition, compared to **1** (9-NH_2, 1.95 μM), all the other 5,6-difluoro derivatives with 9-substituted electron-withdrawing groups (**7a** with 9-NO_2, 15.6 μM; **7b** with 9-CN, 31.25 μM; **7d** with 9-Ac, 15.6 μM; **7e** with 9-NO_2 and 10-Cl, 31.25 μM) were 8–16 fold less active with IC_{50} values ranging from 15.6–31.25 μM. ii). In general, the basic amine functionality at the 6 position significantly enhanced topoisomerase I inhibitory activity. For example, the 6-substituted amine derivatives **11a** with 6-methylpiperazinyl, **11b** with piperazinyl, **11d** with morpholino, **11g** with bipiperidinyl, **11h** with morpholinoethyl, as well as the 6-substituted aminopyrrolidinyl derivatives **16, 17a**, and **17b** demonstrated the most potent topoisomerase I inhibitory activity with IC_{50} values of 0.24–0.97 μM; and within this group, **11d** and **11h** with the morpholino group had an IC_{50} value of 0.97 μM. In contrast, all the other 6-substituted amine derivatives with a more lipophilic side chain, including **11c** with methylpiperidinyl, **11e** with phenethyl, **11f** with adamantanyl, **11i** with cyclohexyl, **11j** with cyclopentyl, **11k** with *n*-hexyl, and **15a** with *t*-Boc-aminopyrrolidinyl, showed weaker topoisomerase I inhibition with IC_{50} values ranging from 3.9 to 15.6 μM. Notably, both 6-substituted aminopyrrolidinyl *S*- and *R*- stereoisomers **17a** and **17b** exhibited the same topoisomerase I inhibitory activity (IC_{50} = 0.48–0.97 μM), suggesting the stereochemistry at the 6 position is not required for topoisomerase I inhibition. iii) Esterification of the carboxylic acid group had little effect on the *E. coli* topoisomerase I inhibitory activity by comparing **6a** and **7a** (IC_{50} = 15.6 μM), **6b** and **7b** (IC_{50} = 31.25 μM), as well as **6c** and **7c** (IC_{50} >125 μM), indicating the ethyl ester functionality is tolerated for topoisomerase I enzyme inhibition. Representative inhibition results of **11a** and **11b** against *E. coli* topoisomerase relaxation activity are shown in Fig. 3.

2.2.2. Selectivity and specificity against other DNA topoisomerase enzymes— In addition, to determine the selectivity and specificity profiles of this class of fluoroquinophenoxazine derivatives, selected compounds were also investigated for the ability to inhibit other DNA topoisomerases including *E. coli* DNA gyrase as well as human topoisomerase I and IIα enzymes. Overall, these compounds were more selective toward *E. coli* topoisomerase I than other enzymes tested. Given that this series of compounds has close structural similarity to quinolone antibiotic class, as such, inhibition against *E. coli* gyrase can be also observed. Specifically, most of the compounds showed 4–64 fold selectivity toward topoisomerase I over DNA gyrase except that the moderately active compound **7e** with the 9-NO_2 and 10-chloro substituents showed less specificity with 2 fold selectivity toward topoisomerase I. With respect to human topoisomerases I and IIα inhibition, these compounds also showed inhibitory activity against both human topoisomerase I (IC_{50} = 3.9–31.25 μM) and topoisomerase IIα (IC_{50} = 0.97–250 μM), with approximate 4–32 fold selectivity. Taken together, compounds **11a** (IC_{50} = 0.48 μM) and **11b** (IC_{50} = 0.24 μM) (Fig. 3) bearing both 9-NH_2 and 6-piperazinyl motifs exhibited the most potent topoisomerase I inhibitory activity with the more favorable selectivity profile (8–64 fold) toward *E. coli* topoisomerase I against all the other enzymes tested.

2.2.3. Cell-based antibacterial activity—In addition to target-based topoisomerase enzyme inhibition, whole cell antibacterial activities of the synthesized compounds were also assessed against a panel of bacterial strains. The results are also shown in Table 1. From these data, the majority of these fluoroquinophenoxazine derivatives exhibited good to excellent antibacterial activity against the membrane permeable *E. coli* strain BAS3023 and Gram-positive *B. subtilis* strain, and were inactive against the wide type *E. coli* strain. Additionally, the antibacterial activity of most fluoroquinophenoxazine derivatives (e.g., **1, 7a, 7c, 9, 10a, 11a–d, 11f–i, 15a, 16**, and **17a–b**) generally correlated with *E. coli* topoisomerase I inhibitory activity, suggesting that the antibacterial basis of these compounds may be in part due to the inhibition of topoisomerase I. The only type IA topoisomerase present in *M. tuberculosis* has recently been validated as an antitubercular target [21]. The topoisomerase I activity has been shown to be essential for viability and infection in a murine model of tuberculosis [21, 22]. To further determine the antituberculosis profile for this chemical class of fluoroquinophenoxazine derivatives, twelve compounds were selected and evaluated against *M. tuberculosis*. Among them, **11g** with the 6-bipiperidinyl lipophilic side chain and **11d** with the 6-morpholino heterocyclic ring system showed the most potent antituberculosis activity with minimum inhibitory concentration (MIC) values of 2.5 and 3.5 μM, respectively. In addition, compared to **11d**, its corresponding 6-piperazinyl structural analogs **11a** with tertiary amine and **11b** with secondary amine functionality was about 2- and 8-fold less active with the MIC values of 7.6 and 29.5 μM, respectively. In contrast, both 6-substituted aminopyrrolidinyl derivatives **17a** (*S*) and **17b** (*R*) with primary amine functionality were not active (MIC > 63.1 μM) against *M. tuberculosis*. These data strongly suggest that the decreased or lost whole cell antituberculosis activity of these compounds are most likely due to their decreased lipophilicity and subsequent cell membrane penetration. Unfortunately, cytotoxicity evaluation of our tested compounds against healthy normal Vero cells showed that they generally had narrow selectivity index, with **11g** (SI = 9.8) being the most promising

compound. It is also worthwhile noting that, one of the most potent topoisomerase I inhibitors, **11a** (IC_{50} = 0.48 μM) bearing the 6-methylpiperazinyl and 9-amino motifs, showed broad spectrum antibacterial activity against all the test bacteria strains with MICs ranging from 0.78 to 7.6 μM (SI = 3.8–37).

2.3. CoMFA analysis

To further understand the structural basis for topoisomerase I inhibitory activity of this set of fluoroquinophenoxazine derivatives, we subsequently performed three dimensional QSAR (3D-QSAR) study using CoMFA analysis [23]. Because of the relatively rigid core structural feature of this class of fluoroquinophenoxazine molecules, we directly applied core structure based alignment to build reliable 3D-QSAR models. The CoMFA study was carried out using a total of 21 compounds (entries 1–21, Table 2). Statistical parameters of the CoMFA model showed a reasonable cross-validated correlation coefficient q^2 of 0.688, indicating a good internal prediction of the model. The CoMFA model also exhibited a conventional correlation coefficient r^2 of 0.806. To evaluate the predictive ability of our developed model, a test set of 7 compounds (entries 22–28, Table 2) which was not included in model generation was subsequently used. The predicative correlation coefficient r^2_{pred} of 0.767 indicates good external predicative ability of the CoMFA model. The experimental and predicted values as well as their residuals from the training and test set molecules are listed in Table 2. The correlation between the predicted and experimental values of all compounds was plotted and the resulting chart is shown in Fig. 4.

The results of the CoMFA model were analyzed and visualized using the standard deviation coefficient (StDev*Coeff) mapping option contoured by steric and electrostatic contributions. In order to probe the structure/activity correlation, the steric and electrostatic contours were mapped onto their aligned chemical structures of these fluoroquinophenoxazine molecules to identify the potential regions in which the molecules would favorably or unfavorably interact with the topoisomerase I enzyme. The representative steric and electrostatic contour maps of the most active compound **11b** and the least active **6c** derived from the CoMFA model are shown in Fig. 5. Briefly, the yellow areas in the steric contour maps indicate regions of steric hindrance to activity, while the green areas indicating steric contribution to potency. From the electrostatic contour maps, the regions in blue indicate positive electrostatic charge potential associated with increased activity, with the red regions show electronegative groups with increased activity.

In Fig. 5A and Fig. 5B, one green contour was found near the piperazinyl moiety of compound **11b** indicating that a moderate steric substituent would be favored at the 6 position of the quinophenoxazine scaffold. This may offer a potential explanation why the 6-substituted amino derivatives were generally more active than the 6-fluoro analogs. In addition, two yellow contours were observed near the 9 position of inactive **6c**, indicating that a steric bulkiness (e.g., NO_2 in **6a** and **7a**, CF_3 in **6c**, and the acetyl group in **7d**) would be disfavored for activity in this area.

The CoMFA electrostatic contour maps are displayed in Fig. 5C and Fig. 5D. A large blue contour was found around the 9 position of compounds **11b** and **6c**, indicating that the presence of electron rich functionalities and positively charged environment at this position

(e.g., NH_2 vs. NO_2, Ac, CN, and CF_3) would be strongly favored for topoisomerase I inhibitory activity. It was also observed that a big red contour region was present around the 2 position of fluoroquinophenoxazine scaffold, suggesting that an electronegative group (e.g., COOH and $COOR_2$) at this position may be required for activity. Finally, two red contours were found at both sides of the fused heterocyclic skeleton of **11b** and **6c**, suggesting that electron deficient functionalities would be favored in those regions.

3. Conclusions

On the basis of a HTS hit compound **1**, a series of fluoroquinophenoxazine analogs were designed, synthesized, and evaluated as topoisomerase IA inhibitors and antibacterial agents. Among the newly produced fluoroquinophenoxazine derivatives, compounds with the 9-NH_2 and/or 6-substituted amine functionalities exhibited good to excellent inhibitory activities against *E. coli* topoisomerase IA with IC_{50} values ranging from 0.24 to 3.9 μM. An illuminating SAR against *E. coli* topoisomerase I has also been obtained. For example, the 6-substituted amino motif significantly enhanced the topoisomerase I inhibition and the 9-NH_2 functionality was the most desirable compared to some other groups evaluated. Notably, **11a** bearing the 6-methylpiperazinyl and 9-amino motifs showed excellent topoisomerase I inhibition (IC_{50} = 0.48 μM) as well as broad spectrum antibacterial activity against all the bacteria strains tested with MICs ranging from 0.78 to 7.6 μM (SI = 3.8–37). In addition, compound **11g** with the 6-bipiperidinyl lipophilic side chain represents a promising antitubercular lead with the most potent antituberculosis activity (MIC = 2.5 μM, SI = 9.8). Finally, CoMFA analysis was performed to investigate the 3D-QSAR. The constructed CoMFA model produced reasonable statistics, with q^2 = 0.688 and r^2 = 0.806. The predictive power of the developed model was obtained using a test set of 7 molecules, giving predictive correlation coefficient r^2_{pred} of 0.767. Collectively, this work has generated valuable SAR and critical understanding for this chemotype class of fluoroquinophenoxazine topoisomerase I inhibitors as antibacterial agents. Our developed CoMFA model can provide important structural insights toward topoisomerase I recognition and guide future structure based design and synthesis of bacterial topoisomerase I inhibitors.

4. Experimental

4.1. General methods for chemistry

All reagents and anhydrous solvents were purchased from Sigma-Aldrich and Fisher Scientific, and were used without further purification. All reactions were monitored either by thin-layer chromatography (TLC) or by analytical high performance liquid chromatography (HPLC) to detect the completion of reactions. TLC was performed using glass plates pre-coated with silica gel (0.25 mm, 60-Å pore size, 230–400 mesh, Sorbent Technologies, GA) impregnated with a fluorescent indicator (254 nm). TLC plates were visualized by exposure to ultraviolet light (UV). Hydrogenation reactions were performed employing domnick hunter NITROX UHP-60H hydrogen generator, USA. Microwave synthesis was performed using Biotage Initiator 8 Exp Microwave System. Compounds were purified by flash column chromatography on silica gel using a Biotage Isolera One system and a Biotage SNAP cartridge. ^1H and ^{13}C NMR spectra were obtained on a Bruker Avance DRX-400 instrument

with chemical shifts (d, ppm) determined using TMS as internal standard. Coupling constants (*J*) are in hertz (Hz). ESI mass spectra in either positive or negative mode were provided by Varian 500-MS IT Mass Spectrometer. High-resolution mass spectra (HRMS) were obtained on an Agilent 6530 Accurate Mass Q-TOF LC/MS. The purity of compounds was determined by analytical HPLC using a Gemini, 3 μm, C18, 110 Å column (50 mm × 4.6 mm, Phenomenex) and a flow rate of 1.0 mL/min. Gradient conditions: solvent A (0.1% trifluoroacetic acid in water) and solvent B (acetonitrile): 0–2.00 min 100% A, 2.00–7.00 min 0–100% B (linear gradient), 7.00–8.00 min 100% B, UV detection at 254 and 220 nm.

4.1.1. 6-Amino-2,3-difluorophenol (2)—2,3-Difluoro-6-nitrophenol (700 mg, 4 mmol) was dissolved in ethanol (5 mL) and palladium on activated carbon (Pd/C) (84.8 mg, 20%) was added. The reaction was stirred at room temperature under H_2 atmosphere (1.0 bar). After 7 h, all starting material was consumed and Pd/C was filtered through Celite. The solvent was evaporated under reduced pressure to afford 6-amino-2,3-difluorophenol (550.5 mg, 95% yield). ^{1}H NMR (400 MHz, $CDCl_3$): δ (ppm) 6.59 (dt, *J* = 9.9, 8.6 Hz, 1H), 6.47–6.31 (m, 1H), 4.27 (br s, 2H). ESI-HRMS: calc. for $C_6H_6F_2NO$ $[M + H]^+$: 146.0412, found: 146.0418.

4.1.2. Diethyl 2-(((3,4-difluoro-2-hydroxyphenyl)amino)methylene)malonate (3)—6-Amino-2,3-difluorophenol (**2**) (550 mg, 3.8 mmol) was dissolved in ethanol (15 mL) and diethyl 2-(ethoxymethylene)malonate (819 mg, 3.8 mmol) was added. The reaction was stirred at room temperature until there was no starting material left. Ethanol was removed and the residue was purified by flash column chromatography on silica gel (EtOAc / hexane = 1 / 3 to 3 / 1) to give product **3** as a brown solid (1.04 g, 87%). ^{1}H NMR (400 MHz, d_6-DMSO): δ (ppm) 10.96 (d, *J* = 14.0 Hz, 1H), 8.45 (d, *J* = 13.9 Hz, 1H), 7.31–7.22 (m, 1H), 6.98–6.86 (m, 1H), 4.20 (q, *J* = 7.1 Hz, 2H), 4.12 (q, *J* = 7.1 Hz, 2H), 1.26 (t, *J* = 7.1 Hz, 3H), 1.24 (t, *J* = 7.1 Hz, 3H). ESI-MS: calc. for $C_{14}H_{14}F_2NO_5$ $[M - H]^-$: 314.3, found: 314.3.

4.1.3. Ethyl 6,7-difluoro-8-hydroxy-4-oxo-1,4-dihydroquinoline-3-carboxylate (4)—Compound **3** (445 mg, 1.4 mmol) was added in a microwave sealed tube. Diphenyl ether (2.5 mL) was added and the tube was sealed with cap. The reaction was then set up at 250 °C in a Biotage Microwave Initiator instrument for 30 min. Hexane was added and the solid was filtered and washed with hexane. The product was then dried and obtained in 80% yield (299.4 mg), which was used for next step without further purification. ^{1}H NMR (400 MHz, d_6-DMSO): δ (ppm) 8.36 (s, 1H), 7.45 (dd, *J* = 10.9, 7.9 Hz, 1H), 4.21 (q, *J* = 7.1 Hz, 2H), 1.27 (t, *J* = 7.1 Hz, 3H). ESI-MS: calc. for $C_{12}H_8F_2NO_4$ $[M - H]^-$: 268.2, found: 268.2.

4.1.4. Ethyl 5,6-difluoro-9-nitro-3-oxo-3H–pyrido[3,2,1-kl]phenoxazine-2-carboxylate (6a)—Compound **4** (269 mg, 1 mmol) and 1-chloro-2,4-dinitrobenzene (202 mg, 1 mmol) were dissolved in DMF (2 mL). $NaHCO_3$ (252 mg, 3 mmol) was added and the reaction was stirred at 100 °C until no starting materials were detected by HPLC. The solid base was removed by filtration through Celite. The filtrate was concentrated and the residue was purified through Biotage reverse phase C18 cartridge to give 220 mg of **6a** as

yellow solid (yield: 57%). ^{1}H NMR (400 MHz, d_6-DMSO): δ (ppm) 9.01 (s, 1H), 8.15 (d, J = 9.6 Hz, 1H), 8.05–8.01 (m, 2H), 7.60–7.54 (m, 1H), 4.27 (q, J = 7.2 Hz, 2H), 1.32 (t, J = 7.2 Hz, 3H); ^{13}C NMR (100 MHz, d_6-DMSO): δ (ppm) 170.4, 163.7, 145.8, 142.7, 138.1, 133.2, 129.4, 124.6, 122.2, 120.8, 117.0, 113.0, 105.4, 105.2, 60.8, 14.2; ESI-MS: calc. for $C_{18}H_{10}F_2N_2O_6Na$ [M + Na]$^+$: 411.3, found: 411.2. ESI-HRMS: calc. for $C_{18}H_{11}F_2N_2O_6$ [M + H]$^+$: 389.0580, found: 389.0582. HPLC purity: 100% (254 nm), t_R: 6.92 min; 100% (220 nm), t_R: 6.92 min. Compounds **6b–e** were prepared according to the experimental procedure above for the preparation of **6a**.

4.1.5. Ethyl 9-cyano-5,6-difluoro-3-oxo-3H–pyrido[3,2,1-kl]phenoxazine-2-carboxylate (6b)—Yellow solid. Yield: 59%. ^{1}H NMR (400 MHz, d_6-DMSO): δ (ppm) 9.04 (s, 1H), 8.11 (d, J = 8.8 Hz, 1H), 7.87 (d, J = 1.6 Hz, 1H), 7.72 (dd, J = 1.6 and 8.8 Hz, 1H), 7.63–7.59 (m, 1H), 4.28 (q, J = 7.2 Hz, 2H), 1.31 (t, J = 7.2 Hz, 3H); ESI-MS: calc. for $C_{19}H_{10}F_2N_2O_4Na$ [M + Na]$^+$: 391.3, found: 391.2. ESI-HRMS: calc. for $C_{19}H_{11}F_2N_2O_4$ [M + H]$^+$: 369.0681, found: 369.0684. HPLC purity: 100% (254 nm), t_R: 6.73 min; 100% (220 nm), t_R: 6.73 min.

4.1.6. Ethyl 5,6-difluoro-3-oxo-9-(trifluoromethyl)-3H–pyrido[3,2,1-kl]phenoxazine-2-carboxylate (6c)—Yellow solid. Yield: 10%. ^{1}H NMR (400 MHz, d_6-DMSO): δ (ppm) 9.05 (s, 1H), 8.12 (d, J = 8.8 Hz, 1H), 7.71 (d, J = 1.6 Hz, 1H), 7.63–7.58 (m, 2H), 4.27 (q, J = 7.2 Hz, 2H), 1.32 (t, J = 7.2 Hz, 3H); ESI-MS: calc. for $C_{19}H_{10}F_5NO_4Na$ [M + Na]$^+$: 434.3, found: 434.1. ESI-HRMS: calc. for $C_{19}H_{11}F_5NO_4$ [M + H]$^+$: 412.0603, found: 412.0603. HPLC purity: 100% (254 nm), t_R: 7.25 min; 100% (220 nm), t_R: 7.25 min.

4.1.7. Ethyl 9-acetyl-5,6-difluoro-3-oxo-3H–pyrido[3,2,1-kl] phenoxazine-2-carboxylate (6d)—Dark yellow solid. Yield: 38%. ^{1}H NMR (400 MHz, d_6-DMSO): δ (ppm) 8.97 (s, 1H), 8.06–7.93 (m, 1H), 7.73 (d, J = 8.4 Hz, 1H), 7.69 (s, 1H), 7.55 (dd, J = 10.2, 8.0 Hz, 1H), 4.27 (q, J = 7.1 Hz, 2H), 2.58 (s, 3H), 1.33 (t, J = 7.1 Hz, 3H). ESI-MS: calc. for $C_{20}H_{13}F_2NNaO_5$ [M + Na]$^+$: 408.3, found: 408.1. HPLC purity: 100% (254 nm), t_R: 6.62 min; 100% (220 nm), t_R: 6.62 min.

4.1.8. Ethyl 10-chloro-5,6-dif luoro-9-nitro-3-oxo-3H–pyrido[3,2,1-kl]phenoxazine-2-carboxylate (6e)—Dark yellow solid. Yield: 40%. ^{1}H NMR (400 MHz, d_6-DMSO): δ (ppm) 9.13 (s, 1H), 8.48 (s, 1H), 8.12 (s, 1H), 7.69–7.60 (m, 1H), 4.30 (q, J = 7.0 Hz, 2H), 1.33 (t, J = 7.1 Hz, 3H). ESI-MS: calc. for $C_{18}H_9ClF_2N_2NaO_6$ [M + Na]$^+$: 445.0, found: 445.1. HPLC purity: 98.5% (254 nm), t_R: 6.92 min; 96.9% (220 nm), t_R: 6.92 min.

4.1.9. 5,6-Difluoro-9-nitro-3-oxo-3H–pyrido[3,2,1-kl]phenoxazine-2-carboxylic acid (7a)—Compound **6a** (180 mg, 0.46 mmol) was dissolved in AcOH (15 mL). Hydrochloric acid (1 N, 2 mL) was added and the reaction was stirred under reflux for 2 h. Upon completion, water was added and yellow solid was precipitated. The solid was collected by filtration and washed with water, then dried and afforded product **7a** (150 mg) as yellow solid in 91% yield. ^{1}H NMR (400 MHz, d_6-DMSO): δ (ppm) 9.36 (s, 1H), 8.42 (d, J = 9.2 Hz, 1H), 8.17 (d, J = 2.8 Hz, 1H), 8.09 (dd, J = 2.4 and 9.2 Hz, 1H), 7.86–7.82

(m, 1H); ESI-MS: calc. for $C_{16}H_7F_2N_2O_6$ $[M + H]^+$: 361.2, found: 361.3. ESI-HRMS: calc. for $C_{16}H_7F_2N_2O_6$ $[M + H]^+$: 361.0267, found: 361.0268. HPLC purity: 100% (254 nm), t_R: 6.79 min; 100% (220 nm), t_R: 6.79 min.

Compounds **7b–e** were prepared according to the experimental procedure above for the preparation of **7a**.

4.1.10. 9-Cyano-5,6-difluoro-3-oxo-3H–pyrido[3,2,1-kl]phenoxazine-2-carboxylic acid (7b)—Yellow solid. Yield: 36%. ^{1}H NMR (400 MHz, d_6-DMSO): δ (ppm) 9.34 (s, 1H), 8.35 (d, J = 8.8 Hz, 1H), 7.98 (d, J = 1.6 Hz, 1H), 7.82 (d, J = 2.4 Hz, 1H), 7.78–7.75 (m, 2H); ESI-MS: calc. for $C_{17}H_7F_2N_2O_4$ $[M + H]^+$: 341.2, found: 341.1. ESI-HRMS: calc. for $C_{17}H_7F_2N_2O_4$ $[M + H]^+$: 341.0368, found: 341.0378. HPLC purity: 95.1% (254 nm), t_R: 6.37 min; 97.7% (220 nm), t_R: 6.37 min.

4.1.11. 5,6-Difluoro-3-oxo-9-(trifluoromethyl)-3H–pyrido[3,2,1-kl]phenoxazine-2-carboxylic acid (7c)—Yellow solid. Yield: 95%. ^{1}H NMR (400 MHz, d_6-DMSO): δ (ppm) 9.35 (s, 1H), 8.37 (d, J = 8.4 Hz, 1H), 7.84–7.79 (m, 2H), 7.65–7.62 (dd, J = 1.2 and 8.8 Hz, 1H); ESI-MS: calc. for $C_{17}H_7F_5NO_4$ $[M + H]^+$: 384.2, found: 384.1. ESI-HRMS: calc. for $C_{17}H_7F_5NO_4$ $[M + H]^+$: 384.0290, found: 384.0293. HPLC purity: 100% (254 nm), t_R: 7.15 min; 100% (220 nm), t_R: 7.15 min.

4.1.12. 9-Acetyl-5,6-difluoro-3-oxo-3H–pyrido[3,2,1-kl] phenoxazine-2-carboxylic acid (7d)—Yellow solid. Yield: 62%. ^{1}H NMR (400 MHz, d_6-DMSO): δ (ppm) 9.36 (s, 1H), 8.30 (d, J = 11.2 Hz, 1H), 7.85–7.80 (m, 3H), 2.63 (s, 3H); ESI-MS: calc. for $C_{18}H_{10}F_2NO_5$ $[M + H]^+$: 358.3, found: 358.2. ESI-HRMS: calc. for $C_{18}H_{10}F_2NO_5$ $[M + H]^+$: 358.0522, found: 358.0521. HPLC purity: 97.3% (254 nm), t_R: 6.70 min; 97.2% (220 nm), t_R: 6.70 min.

4.1.13. 10-Chloro-5,6-difluoro-9-nitro-3-oxo-3H–pyrido[3,2,1-kl]phenoxazine-2-carboxylic acid (7e)—Brown solid. Yield: 39%. ^{1}H NMR (400 MHz, d_6-DMSO): δ (ppm) 9.43 (s, 1H), 8.74 (s, 1H), 8.18 (s, 1H), 7.83–7.79 (m, 1H); ESI-MS: calc. for $C_{16}H_6ClF_2N_2O_6$ $[M + H]^+$: 394.7, found: 394.9. ESI-HRMS: calc. for $C_{16}H_6F_2N_2ClO_6$ $[M + H]^+$: 394.9877, found: 394.9879. HPLC purity: 95.4% (254 nm), t_R: 6.90 min; 97.0% (220 nm), t_R: 6.90 min.

4.1.14. 9-Amino-5,6-difluoro-3-oxo-3H–pyrido[3,2,1-kl]phenoxazine-2-carboxylic acid (1)—Compound **7a** (150 mg, 0.42 mmol) was added to a mixture of AcOH / HCl (1 / 1). $SnCl_2$ (236 mg, 1.25 mmol) was added and the reaction was stirred under reflux for 2 h. No starting material was observed in the reaction and then water was added. The large amount of solid precipitated and was collected by filtration. Product **1** was obtained in 86% yield (236 mg) as yellow solid. ^{1}H NMR (400 MHz, d_6-DMSO): δ (ppm) 9.08 (s, 1H), 7.79 (d, J = 9.2 Hz, 1H), 7.76–7.73 (m, 1H), 6.48 (dd, J = 2.4 and 9.2 Hz, 1H), 6.43 (d, J = 2.4 Hz, 1H); ESI-MS: calc. for $C_{16}H_9F_2N_2O_4$ $[M + H]^+$: 331.3, found: 331.1. ESI-HRMS: calc. for $C_{16}H_9F_2N_2O_4$ $[M + H]^+$: 331.0525, found: 331.0526. HPLC purity: 100% (254 nm), t_R: 6.47 min; 100% (220 nm), t_R: 6.47 min.

4.1.15. Ethyl-5-fluoro-6-(4-m ethylpiperazin-1-yl)-9-nitro-3-oxo-3H–pyrido[3,2,1-kl]phenoxazine-2-carboxylate (9)—Compound **6a** (159 mg, 0.4 mmol) was dissolved in pyridine (1 mL) and 1-methylpiperazine (120 mg, 1.2 mmol) was added. The reaction was heated to 110 °C until no starting material was observed. Pyridine was removed under reduced pressure and the residue was purified by flash column chromatography on silica gel (MeOH / CH_2Cl_2 = 1 / 19), affording product **9** (100.1 mg) in 53% yield as orange solid. ^{1}H NMR (400 MHz, d_6-DMSO): δ (ppm) 8.87 (d, J = 1.6 Hz, 1H), 8.04–7.97 (m, 2H), 7.87 (t, J = 1.2 Hz, 1H), 7.32 (dd, J = 1.2 and 8.0 Hz, 2H), 4.25 (q, J = 7.2 Hz, 2H), 3.34 (s, 4H), 3.27 (s, 4H), 2.27 (s, 3H), 1.32 (t, J = 7.2 Hz, 3H); ESI-MS: calc. for $C_{23}H_{22}FN_4O_6$ $[M + H]^+$: 469.4, found: 469.3. HPLC purity: 100% (254 nm), t_R: 5.48 min; 100% (220 nm), t_R: 5.48 min.

4.1.16. 5-Fluoro-6-(4-methylpiperazin-1-yl)-9-nitro-3-oxo-3H–pyrido[3,2,1-kl]phenoxazine-2-carboxylic acid (10a)—Compound **7a** (108 mg, 0.3 mmol) was dissolved in pyridine (4 mL), and then the reaction was heated to 90 °C. 1-Methylpiperazine (100 μL, 0.9 mmol) was added and the reaction was stirred under nitrogen atmosphere until there was no starting material. Upon completion, pyridine was removed under reduced pressure and the residue was dissolved in ethanol (10 mL) and heated under reflux for additional 30 min. The solid was filtered and washed with water, then dried to obtain product **10a** (60 mg) in 45 % yield as yellow solid. ^{1}H NMR (400 MHz, d_6-DMSO): δ (ppm) 9.18 (s, 1H), 8.29 (d, J = 8.0 Hz, 1H), 8.02–7.99 (m, 2H), 7.53 (d, J = 12.6 Hz, 1H), 3.30 (br s, overlapping with H_2O peak, 4H), 2.57 (br s, 4H), 2.32 (s, 3H); ESI-MS: calc. for $C_{21}H_{18}FN_4O_6$ $[M + H]^+$: 441.4, found: 441.4. ESI-MS: calc. for $C_{21}H_{18}FN_4O_6$ $[M + H]^+$: 441.1205, found: 441.1216. HPLC purity: 100% (254 nm), t_R: 5.37 min; 100% (220 nm), t_R: 5.37 min. Compounds **10b** and **11a–k** were prepared following the similar procedure for the preparation of **10a**.

4.1.17. 5-Fluoro-9-nitro-3-oxo-6-(piperazin-1-yl)-3H–pyrido[3,2,1-kl]phenoxazine-2-carboxylic a ci d (10b)—Yellow solid. Yield: 84%. ^{1}H NMR (400 MHz, d_6-DMSO): δ (ppm) 8.94 (s, 1H), 7.66 (d, J = 8.8 Hz, 1H), 7.45 (d, J = 12.0 Hz, 1H), 6.43–6.36 (m, 2H), 3.22 (s, 4H), 2.87 (s, 4H); ESI-MS: calc. for $C_{20}H_{16}FN_4O_6$ $[M + H]^+$: 427.4, found: 427.2. ESI-HRMS: calc. for $C_{20}H_{16}FN_4O_6$ $[M + H]^+$: 427.1048, found: 427.1041. HPLC purity: 100% (254 nm), t_R: 5.36 min; 100% (220 nm), t_R: 5.36 min.

4.1.18. 9-Amino-5-fluoro-6-(4-methylpiperazin-1-yl)-3-oxo-3H–pyrido[3,2,1-kl]phenoxazine-2-carboxylic acid (11a)—Yellow solid. Yield: 48%. ^{1}H NMR (400 MHz, d_6-DMSO): δ (ppm) 8.94 (s, 1H), 7.65 (d, J = 9.2 Hz, 1H), 7.45 (d, J = 12.0 Hz, 1H), 6.43–6.36 (m, 2H), 5.77 (s, 2H), 3.31 (s, 4H), 2.57 (s, 4H), 2.32 (s, 3H); ESI-MS: calc. for $C_{21}H_{20}FN_4O_4$ $[M + H]^+$: 411.4, found: 411.2. ESI-MS: calc. for $C_{21}H_{20}FN_4O_4$ $[M + H]^+$: 411.1463, found: 411.1466. HPLC purity: 100% (254 nm), t_R: 5.22 min; 100% (220 nm), t_R: 5.22 min.

4.1.19. 9-Amino-5-fluoro-3-oxo-6-(piperazin-1-yl)-3H–pyrido[3,2,1-kl]phenoxazine-2-carboxylic acid (11b)—Yellow solid. Yield: 97%. ^{1}H NMR (400 MHz, d_6-DMSO): δ (ppm) 8.97 (s, 1H), 7.68 (d, J = 9.2 Hz, 1H), 7.48 (d, J = 12.4 Hz, 1H),

6.44–6.38 (m, 2H), 5.77 (s, 2H), 3.22 (s, 4H), 2.86 (s, 4H); ESI-MS: calc. for $C_{20}H_{18}FN_4O_4$ $[M + H]^+$: 397.4, found: 397.2. ESI-HRMS: calc. for $C_{20}H_{18}FN_4O_4$ $[M + H]^+$: 397.1307, found: 397.1303. HPLC purity: 100% (254 nm), t_R: 5.20 min; 100% (220 nm), t_R: 5.20 min.

4.1.20. 9-Amino-5-fluoro-6-(4-methylpiperidin-1-yl)-3-oxo-3H–pyrido[3,2,1-kl]phenoxazine-2-carboxylic acid (11c)—Yellow solid. Yield: 33%. ^{1}H NMR (400 MHz, d_6-DMSO): δ (ppm) 8.92 (s, 1H), 7.63 (d, J = 8.0 Hz, 1H), 7.43 (d, J = 11.6 Hz, 1H), 6.42–6.36 (m, 2H), 5.75 (s, 2H), 3.13 (t, J = 10.8 Hz, 2H), 1.71 (d, J = 11.2 Hz, 2H), 1.57 (s, 1H), 1.32–1.26 (m, 2H), 0.98 (s, 3H); ^{13}C NMR (100 MHz, d_6-DMSO): δ (ppm) 175.4, 166.4, 150.7, 144.6, 138.5, 136.0, 131.7, 125.3, 119.6, 119.5, 117.6, 112.2, 111.1, 107.0, 104.0, 101.2, 51.1, 35.1, 30.6, 22.5; ESI-MS: calc. for $C_{22}H_{21}FN_3O_4$ $[M + H]^+$: 410.4, found: 410.2. ESI-HRMS: calc. for $C_{22}H_{21}FN_3O_4$ $[M + H]^+$: 410.1511, found: 410.1510. HPLC purity: 100% (254 nm), t_R: 6.38 min; 100% (220 nm), t_R: 6.38 min.

4.1.21. 9-Amino-5-fluoro-6-morpholino-3-oxo-3H–pyrido[3,2,1-kl]phenoxazine-2-carboxylic acid (11d)—Yellow solid. Yield: 71%. ^{1}H NMR (400 MHz, d_6-DMSO): δ (ppm) 8.93 (s, 1H), 7.64 (d, J = 8.8 Hz, 1H), 7.45 (d, J = 12.0 Hz, 1H), 6.43–6.37 (m, 2H), 5.75 (s, 2H), 3.69 (s, 4H), 3.28 (s, 4H); ESI-MS: calc. for $C_{20}H_{17}FN_3O_5$ $[M + H]^+$: 398.4, found: 398.2. ESI-HRMS: calc. for $C_{20}H_{17}FN_3O_5$ $[M + H]^+$: 398.1147, found: 398.1146. HPLC purity: 100% (254 nm), t_R: 6.38 min; 100% (220 nm), t_R: 6.38 min.

4.1.22. 9-Amino-5-fluoro-3-oxo-6-(phenethylamino)-3H–pyrido[3,2,1-kl]phenoxazine-2-carboxylic acid (11e)—Yellow solid. Yield: 55%. ^{1}H NMR (400 MHz, d_6-DMSO): δ (ppm) 8.90 (s, 1H), 7.61 (d, J = 9.2 Hz, 1H), 7.45 (d, J = 13.2 Hz, 1H), 7.29–7.18 (m, 5H), 6.43–6.37 (m, 2H), 6.15 (br s, 1H), 5.76 (br s, 2H), 3.68–3.61 (m, 2H), 2.89–2.85 (m, 2H); ESI-MS: calc. for $C_{24}H_{18}FN_3O_4$ $[M + H]^+$: 432.4, found: 432.1. ESI-HRMS: calc. for $C_{24}H_{19}FN_3O_4$ $[M + H]^+$: 432.1354, found: 432.1362. HPLC purity: 100% (254 nm), t_R: 7.07 min; 100% (220 nm), t_R: 7.07 min.

4.1.23. 6-(((3s,5s,7s)-Adamantan-1-yl)amino)-9-amino-5-fluoro-3-oxo-3H–pyrido[3,2,1-kl]phenoxazine-2-carboxylic acid (11f)—Brown solid. Yield: 29%. ^{1}H NMR (400 MHz, d_6-DMSO): δ (ppm) 9.00 (s, 1H), 7.71 (d, J = 9.1 Hz, 1H), 7.54 (d, J = 10.7 Hz, 1H), 6.50–6.38 (m, 2H), 5.81 (s, 2H), 4.34 (s, 1H), 2.09–2.04 (m, 3H), 1.85 (s, 6H), 1.65–1.55 (m, 6H). ESI-MS: calc. for $C_{26}H_{23}FN_3O_4$ $[M - H]^+$: 460.2, found: 460.0. HPLC purity: 85.2% (254 nm), t_R: 7.41 min; 91.1% (220 nm), t_R: 7.41 min.

4.1.24. 6-([1,4'-Bipiperidin]-1'-yl)-9-amino-5-fluoro-3-oxo-3H–pyrido[3,2,1-kl]phenoxazine-2-carboxylic acid (11g)—Yellow solid. Yield: 64%. ^{1}H NMR (400 MHz, d_6-DMSO): δ (ppm) 8.98 (s, 1H), 7.68 (d, J = 4.0 Hz, 1H), 7.49 (d, J = 9.6 Hz, 1H), 6.45–6.41 (m, 2H), 5.77 (br s, 2H), 3.20–3.15 (m, 1H), 1.84–1.82 (m, 3H), 1.64–1.41 (m, 14H), 1.06–1.04 (m, 1H); ESI-MS: calc. for $C_{26}H_{28}FN_4O_4$ $[M + H]^+$: 479.5, found: 479.3. ESI-HRMS: calc. for $C_{26}H_{28}FN_4O_4$ $[M + H]^+$: 479.2089, found: 479.2093. HPLC purity: 100% (254 nm), t_R: 5.53 min; 100% (220 nm), t_R: 5.53 min.

4.1.25. 9-Amino-5-fluoro-6-((2-morpholinoethyl)amino)-3-oxo-3H–pyrido[3,2,1-kl]phenoxazine-2-carboxylic acid (11h)—Yellow solid. Yield: 74%. ^{1}H NMR (400

MHz, d_6-DMSO): δ (ppm) 8.90 (s, 1H), 8.55 (s, 1H), 7.46 (d, J = 6.0 Hz, 1H), 7.39–7.34 (m, 2H), 6.42–6.37 (m, 2H), 5.95 (s, 1H), 5.78 (br s, 2H), 2.57 (s, 2H), 2.44 (br s, 6H); ESI-MS: calc. for $C_{22}H_{22}FN_4O_5$ $[M + H]^+$: 441.4, found: 441.3. ESI-MS: calc. for $C_{22}H_{22}FN_4O_5$ $[M + H]^+$: 441.1569, found: 441.1579. HPLC purity: 97.2% (254 nm), t_R: 5.22 min; 99.3% (220 nm), t_R: 5.22 min.

4.1.26. 9-Amino-6-(cyclohexylamino)-5-fluoro-3-oxo-3H–pyrido[3,2,1-kl]phenoxazine-2-carboxylic acid (11i)—Brown solid. Yield: 74%. ^{1}H NMR (400 MHz, d_6-DMSO): δ (ppm) 8.86 (s, 1H), 7.58–7.56 (m, 1H), 7.43–7.40 (m, 1H), 6.40 (s, 1H), 5.72 (s, 2H), 5.40–5.38 (m, 1H), 1.92 (s, 3H), 1.73–1.67 (m, 3H), 1.31–1.22 (m, 6H); ESI-MS: calc. for $C_{22}H_{21}FN_3O_4$ $[M + H]^+$: 410.4, found: 410.3. ESI-HRMS: calc. for $C_{22}H_{21}FN_3O_4$ $[M + H]^+$: 410.1511, found: 410.1494. HPLC purity: 100% (254 nm), t_R: 7.27 min; 100% (220 nm), t_R: 7.27 min.

4.1.27. 9-Amino-6-(cyclopentylamino)-5-fluoro-3-oxo-3H–pyrido[3,2,1-kl]phenoxazine-2-carboxylic acid (11j)—Black solid. Yield: 63%. ^{1}H NMR (400 MHz, d_6-DMSO): δ (ppm) 8.91 (s, 1H), 7.62 (d, J = 8.8 Hz, 1H), 7.47 (d, J = 12.4 Hz, 1H), 6.46–6.41 (m, 2H), 5.73 (s, 2H), 5.53 (d, J = 2.4 Hz, 1H), 4.30 (s, 1H), 1.93 (br s, 4H), 1.73 (br s, 4H); ESI-MS: calc. for $C_{21}H_{19}FN_3O_4$ $[M + H]^+$: 396.4, found: 396.1. ESI-HRMS: calc. for $C_{21}H_{19}FN_3O_4$ $[M + H]^+$: 396.1354, found: 396.1358. HPLC purity: 96.7% (254 nm), t_R: 7.07 min; 96.0% (220 nm), t_R: 7.06 min.

4.1.28. 9-Amino-5-fluoro-6-(hexylamino)-3-oxo-3H–pyrido[3,2,1-kl]phenoxazine-2-carboxylic acid (11k)—Yellow solid. Yield: 49%. ^{1}H NMR (400 MHz, d_6-DMSO): δ (ppm) 8.88 (s, 1H), 7.64 (s, 1H), 7.44 (s, 1H), 6.56–6.36 (m, 2H), 5.88–5.50 (m, 2H), 1.57 (s, 2H), 1.27 (s, 7H), 0.84 (s, 4H); ESI-MS: calc. for $C_{22}H_{23}FN_3O_4$ $[M + H]^+$: 412.4, found: 412.2. ESI-HRMS: calc. for $C_{22}H_{23}FN_3O_4$ $[M + H]^+$: 412.1667, found: 412.1672. HPLC purity: 100% (254 nm), t_R: 7.47 min; 100% (220 nm), t_R: 7.47 min.

4.1.29. 9-acetamido-5,6-difluoro-3-oxo-3H–pyrido[3,2,1-kl]phenoxazine-2-carboxylic acid (12)—To the solution of **1** (33 mg, 0.1 mmol) and pyridine (1 mL), acetic anhydride (12.2 mg, 0.12 mmol) was added. The reaction was stirred at 80 °C for 3 h, then at 100 °C until no starting material was detected by HPLC. The solid was filtered and dried to give 34.1 mg of **12** in 92% yield. Yellow solid. ^{1}H NMR (400 MHz, d_6-DMSO): δ (ppm) 10.31 (s, 1H), 9.20 (s, 1H), 8.05 (d, J = 9.2 Hz, 1H), 7.78 (t, J = 8.0 Hz, 1H), 7.66 (s, 1H), 7.29 (d, J = 7.6 Hz, 1H), 2.06 (s, 3H); ESI-MS: calc. for $C_{18}H_{11}F_2N_2O_5$ $[M + H]^+$: 373.3, found: 373.2. ESI-MS: calc. for $C_{18}H_{11}F_2N_2O_5$ $[M + H]^+$: 373.0631, found: 373.0638. HPLC purity: 98.6% (254 nm), t_R: 6.42 min; 99.1% (220 nm), t_R: 6.42 min. Compounds **14** and **15a–b** were prepared at 70 °C following the similar procedure for the preparation of **10a**

4.1.30. (S)-9-amino-6-(3-((tert-butoxycarbonyl)amino)pyrrolidin-1-yl)-5-fluoro-3-oxo-3H–pyrido[3,2,1-kl]phenoxazine-2-carboxylic acid (15a)—Yellow solid. Yield: 86%. ^{1}H NMR (400 MHz, d_6-DMSO): δ (ppm) 8.77 (s, 1H), 7.49 (d, J = 9.6 Hz, 1H), 7.31 (d, J = 14.0 Hz, 1H), 7.17 (d, J = 5.6 Hz, 1H), 6.38 (dd, J = 2.4 and 9.2 Hz, 2H), 6.29 (d, J = 2.0 Hz, 1H), 5.67 (s, 2H), 3.82–3.80 (m, 5H), 2.05–2.04 (m, 1H), 1.83 (br s, 1H), 1.38 (s, 9H); ESI-MS: calc. for $C_{25}H_{26}FN_4O_6$ $[M + H]^+$: 497.5, found: 497.3. ESI-HRMS: calc. for

$C_{25}H_{26}FN_4O_6$ [M + H]$^+$: 497.1831, found: 497.1831. HPLC purity: 100% (254 nm), t_R: 6.94 min; 100% (220 nm), t_R: 6.94 min.

4.1.31. (S)-6-(3-aminopyrroli din-1-yl)-5-fluoro-9-nitro-3-oxo-3H–pyrido[3,2,1-kl] phenoxazine-2-carboxyl ic acid (16)—Compound **16** was prepared following the same procedure for the synthesis of **7**. Brown solid. Yield: 32% (two steps). ^{1}H NMR (400 MHz, d_6-DMSO): δ (ppm) 9.10 (s, 1H), 8.41 (s, 2H), 8.25 (d, J = 9.3 Hz, 1H), 8.09 (s, 1H), 8.01 (d, J = 7.2 Hz, 1H), 7.48 (d, J = 13.6 Hz, 1H), 4.07 – 3.74 (m, 5H), 2.28 (s, 1H), 2.08 (s, 1H). ESI-MS: calc. for $C_{20}H_{16}FN_4O_6$ [M + H]$^+$: 427.4, found: 427.1. HPLC purity: 100% (254 nm), t_R: 5.45 min; 100% (220 nm), t_R: 5.46 min.

4.1.32. (S)-9-amino-6-(3-aminopyrrolidin-1-yl)-5-fluoro-3-oxo-3H–pyrido[3,2,1-kl]phenoxazine-2-carboxylic acid (17a)—Compound **15a** (85 mg, 0.17 mmol) was dissolved in 10 mL of hydrochloric acid (1 N). The reaction was stirred under reflux for 2.5 h. The solvent was removed and ethanol (10 mL) was added. The mixture was heated under reflux for 30 min. The solid was collected by filtration and dried to yield 52 mg of **17a** in 78% yield. Yellow solid. ^{1}H NMR (400 MHz, d_6-DMSO): δ (ppm) 8.94 (s, 1H), 8.24 (s, 3H), 7.65 (d, J = 9.2 Hz, 1H), 7.50 (d, J = 13.6 Hz, 1H), 6.46–6.40 (m, 2H), 3.99–3.85 (m, 5H), 2.34–2.26 (m, 1H), 2.09–1.98 (m, 1H); ESI-MS: calc. for $C_{20}H_{18}FN_4O_4$ [M + H]$^+$: 397.4, found: 397.1. ESI-MS: calc. for $C_{20}H_{18}FN_4O_4$ [M + H]$^+$: 397.1307, found: 397.1298. HPLC purity: 100% (254 nm), t_R: 5.20 min; 100% (220 nm), t_R: 5.20 min.

4.1.33. (R)-9-amino-6-(3-aminopyrrolidin-1-yl)-5-fluoro-3-oxo-3H–pyrido[3,2,1-kl]phenoxazine-2-carboxylic acid (17b)—Compound **17b** was prepared using the same procedure for the synthesis of **17a**. Brown solid. Yield: 48% (two steps). ^{1}H NMR (400 MHz, d_6-DMSO): δ (ppm) 8.88 (s, 1H), 8.31 (s, 3H), 7.59 (d, J = 9.2 Hz, 1H), 7.43 (d, J = 13.2 Hz, 1H), 6.42 (d, J = 9.2 Hz, 1H), 6.38 (s, 1H), 3.98–3.88 (m, 2H), 3.73–3.68 (m, 3H), 2.30–2.25 (m, 1H), 2.06–2.03 (m, 1H); ESI-MS: calc. for $C_{20}H_{18}FN_4O_4$ [M + H]$^+$: 397.4, found: 397.2. ESI-HRMS: calc. for $C_{20}H_{18}FN_4O_4$ [M + H]$^+$: 397.1307, found: 397.1302. HPLC purity: 100% (254 nm), t_R: 5.24 min; 100% (220 nm), t_R: 5.24 min.

4.2. Target-based biochemical assays

Topoisomerase enzymes—Recombinant *E. coli* topoisomerase I and gyrase expressed in *E. coli* were purified as described previously [24, 25]. Human topoisomerase I and topoisomerase IIα were purchased from TopoGen (Buena vista, CO, USA).

4.2.1. E. coli topoisomerase I relaxation activity inhibition assay—The relaxation activity of *E. coli* topoisomerase I was assayed in a buffer containing 10 mM Tris-HCl, pH 8.0, 50 mM NaCl, 0.1 mg/mL gelatin, and 0.5 mM $MgCl_2$. Half microliter from the appropriate stock solutions of compounds dissolved in the solvent (DMSO) or the solvent alone (control) was mixed with 9.5 μL of the reaction buffer containing 10 ng of enzyme before the addition of 10 μL of reaction buffer containing 200 ng of supercoiled pBAD/Thio plasmid DNA purified by cesium chloride gradient as substrate. Following incubation at 37 °C for 30 min, the reactions were terminated by the addition of 4 μL of a stop buffer (50% glycerol, 50 mM EDTA, and 0.5% (v/v) bromophenol blue), and analyzed by agarose

gel electrophoresis. The gels were stained in ethidium bromide and photographed under UV light.

4.2.2. DNA gyrase supercoiling inhibition assay—DNA gyrase supercoiling assays were carried out by mixing the compounds and the enzyme in a similar manner as above (EcTopI relaxation inhibition assay) but in a gyrase assay buffer (35 mM Tris-HCl, 24 mM KCl, 4 mM $MgCl_2$, 2 mM DTT, 1.75 mM ATP, 5 mM spermidine, 0.1 mg/mL BSA, 6.5 % glycerol at pH 7.5), followed by the addition of 300 ng of relaxed covalently closed circular DNA (New England Biolabs, Ipswich, MA, USA) to a final reaction volume of 20 μL. The samples were incubated at 37 °C for 30 minutes before being terminated by the addition of a buffer containing 5% SDS, 0.25% bromophenol blue, and 25% glycerol. The reactions were then analyzed by agarose gel electrophoresis.

4.2.3. Human topoisomerase I relaxation inhibition assay—Human topoisomerase I relaxation assays were carried out with 0.5 U of enzyme in reaction buffer supplied by the manufacturer. The enzyme was mixed with the indicated concentration of compound dissolved before 200 ng of supercoiled pBAD/Thio plasmid DNA was added in the same buffer, for a final volume of 20 μL. Following incubation at 37 °C for 30 minutes, the reactions were terminated with a buffer containing 5% SDS, 0.25% bromophenol blue, and 25% glycerol, and analyzed by agarose gel electrophoresis.

4.2.4. Human topoisomerase IIα decatenation inhibition assay—Human Topoisomerase IIα assays were carried out by adding the compounds to 185 ng of kinetoplast DNA (kDNA, from TopoGen) in the buffer supplied by the manufacturer before the addition of 2 U of the enzyme. The samples were incubated for 15 minutes at 37 °C before the addition of 4 μL of a stop buffer containing 5% sarkosyl, 0.25% bromophenol blue, and 25% glycerol. The reactions were then analyzed by electrophoresis in 1% agarose gels containing 0.5 μg/mL ethidium bromide before being photographed under UV light.

4.3. Cell-based assays

The minimum inhibitory concentrations (MIC) of the compounds were determined against *E. coli* and *B. subtilis* in cation-adjusted Mueller-Hinton Broth according to standard microdilution protocol [26].

MICs of compounds against *M. tuberculosis* were determined by a modified microplate Alamar blue assay (MABA) [27]. Vero cell cytotoxicity assay was performed as previously described [27].

4.4. CoMFA modeling

4.4.1. Dataset—All the synthesized and tested fluoroquinophenoxazine derivatives were used for CoMFA study. The topoisomerase I inhibitory activity (IC_{50}, μM) from biochemical enzyme assay was converted to pIC_{50} values for correlation purpose ($pIC_{50} = – \log IC_{50}$). The total compound set is divided into two subsets: a training set of 21 compounds for generating 3D-QSAR models and a test set of 7 compounds for validating the quality of the model (Table 2). The compound selections of training and test sets were done manually so

that compounds ranging from weak, moderate, to strong topoisomerase I inhibitory activities were present in both sets and were in approximately equal proportions.

4.4.2. Conformational model analysis and molecular alignment—In the 3D-QSAR studies, alignment rule and biological conformation selection are two important factors to construct reliable models. For both training and test set molecules, conformational models representing their available conformational space were calculated. All the molecules were subjected to produce a maximum of 255 conformations within 20 kcal/mol in energy from global minimum. Due to the relatively rigid structural feature of these molecules, the core structure of quinophenoxazine was used for the alignment.

4.4.3. CoMFA model generation—CoMFA was performed using the QSAR module of SYBYL-X [28]. The steric and electrostatic field energies were calculated using the Lennard-Jones and the Coulomb potentials, respectively, with a 1/r distance-dependent dielectric constant in all intersections of a regularly spaced (0.2 nm) grid. The electrostatic fields were computed using Gasteiger-Huckel charge calculation methods. A sp^3 hybridized carbon atom with a radius of 1.53 Å and a charge of +1.0 was used as a probe to calculate the steric and electrostatic energies between the probe and the molecules using the Tripos force field. The standard parameters implemented in SYBYL-X were used. The truncation for both steric and electrostatic energies was set to 30 kcal/mol.

4.4.4. Partial least square (PLS) analysis—PLS methodology [29] was used for 3D-QSAR analysis. The cross-validation analysis [30, 31] was performed using the leave one out (LOO) methods in which one compound is removed from the dataset and its activity is then predicted using the model derived from the rest of the dataset. The cross validated r^2 that resulted in the optimum number of components and the lowest standard error of prediction were considered for further analysis. To speed up the analysis and reduce noise, a minimum filter value of 2.00 kcal/mol was used. A final analysis was performed to calculate conventional r^2 using the optimum number of components obtained from the cross-validation analysis.

Supplementary Material

Refer to Web version on PubMed Central for supplementary material.

Acknowledgments

This project was supported in part by the National Institutes of Health grants (P20GM103466 and R15AI092315 to DS, R01AI069313 to YT). MICs against *M. tuberculosis* and Vero cell cytotoxicity were provided by the service available at the Institute for Tuberculosis Research at University of Illinois at Chicago. NSC648059 was provided by the NCI Developmental Therapeutics Program.

Abbreviations

SAR	structure-activity relationship
HTS	high-throughput screening
QSAR	quantitative structure-activity relationship

CoMFA	comparative molecular field analysis
MIC	minimum inhibitory concentration
SI	selectivity index
3D-QSAR	three dimensional QSAR
PA	predicted activity
TLC	thin-layer chromatography
HPLC	high performance liquid chromatography
MABA	microplate Alamar blue assay
PLS	partial least square
LOO	leave one out

References

1. Wang JC. Cellular roles of DNA topoisomerases: a molecular perspective. Nat. Rev. Mol. Cell Biol. 2002; 3:430–440. [PubMed: 12042765]
2. Vos SM, Tretter EM, Schmidt BH, Berger JM. All tangled up: how cells direct, manage and exploit topoisomerase function. Nat. Rev. Mol. Cell Biol. 2011; 12:827–841. [PubMed: 22108601]
3. Olivier S, Qasim AK, Kurt WK, Yves P. Apoptosis induced by topoisomerase inhibitors. Curr. Med Chem. Anticancer Agents. 2003; 3:271–290. [PubMed: 12769773]
4. Pommier Y, Leo E, Zhang H, Marchand C. DNA topoisomerases and their poisoning by anticancer and antibacterial drugs. Chem. Biol. 2010; 17:421–433. [PubMed: 20534341]
5. Pommier Y. Drugging topoisomerases: Lessons and challenges. ACS Chem. Biol. 2013; 8:82–95. [PubMed: 23259582]
6. Tse-Dinh Y-C. Targeting bacterial topoisomerase I to meet the challenge of finding new antibiotics. Future Med. Chem. 2015; 7:459–471. [PubMed: 25875873]
7. Tse-Dinh Y-C. Bacterial topoisomerase I as a target for discovery of antibacterial compounds. Nucl. Acids Res. 2009; 37:731–737. [PubMed: 19042977]
8. Lin H, Annamalai T, Bansod P, Tse-Dinh Y-C, Sun D. Synthesis and antibacterial evaluation of anziaic acid and its analogues as topoisomerase I inhibitors. MedChemComm. 2013; 4:1613–1618.
9. Feng L, Maddox MM, Alam MZ, Tsutsumi LS, Narula G, Bruhn DF, Wu X, Sandhaus S, Lee RB, Simmons CJ, Tse-Dinh Y-C, Hurdle JG, Lee RE, Sun D. Synthesis, structure-activity relationship studies, and antibacterial evaluation of 4-chromanones and chalcones, as well as olympicin A and derivatives. J. Med. Chem. 2014; 57:8398–8420. [PubMed: 25238443]
10. Karl D, Muhammad M. Fluoroquinolones: Action and resistance. Curr. Top. Med. Chem. 2003; 3:249–282. [PubMed: 12570763]
11. Rádl S, Zikán V. Synthesis and antimicrobial activity of some 3-oxo-3*H*–pyrido[3,2,1-*kl*]phenoxazine-2-carboxylic acids. Collect. Czech. Chem. Commun. 1989; 54:506–515.
12. Chu DTW, Maleczka RE. Synthesis of 4-oxo-4H–quino[2,3,4-i,j][1,4]-benoxazine-5-carboxylic acid derivatives. J. Heterocyclic Chem. 1987; 24:453–456.
13. Kang D-H, Kim J-S, Jung M-J, Lee E-S, Jahng Y, Kwon Y, Na Y. New insight for fluoroquinophenoxazine derivatives as possibly new potent topoisomerase I inhibitor. Bioorg. Med. Chem. Lett. 2008; 18:1520–1524. [PubMed: 18178085]
14. Permana PA, Snapka RM, Shen LL, Chu DTW, Clement JJ, Plattner JJ. Quinobenoxazines: A class of novel antitumor quinolones and potent mammalian DNA topoisomerase II catalytic inhibitors. Biochemistry. 1994; 33:11333–11339. [PubMed: 7727384]

15. Fan J-Y, Sun D, Yu H, Kerwin SM, Hurley LH. Self-assembly of a quinobenzoxazine-Mg^{2+} complex on DNA: A new paradigm for the structure of a drug-DNA complex and implications for the structure of the quinolone bacterial gyrase-DNA complex. J. Med. Chem. 1995; 38:408–424. [PubMed: 7853333]
16. Duan W, Rangan A, Vankayalapati H, Kim M-Y, Zeng Q, Sun D, Han H, Fedoroff OY, Nishioka D, Rha SY, Izbicka E, Von Hoff DD, Hurley LH. Design and synthesis of fluoroquinophenoxazines that interact with human telomeric G-quadruplexes and their biological effects. Mol. Cancer Ther. 2001; 1:103–120. [PubMed: 12467228]
17. Smith CJ, Ali A, Chen L, Hammond ML, Anderson MS, Chen Y, Eveland SS, Guo Q, Hyland SA, Milot DP, Sparrow CP, Wright SD, Sinclair PJ. 2-Arylbenzoxazoles as CETP inhibitors: Substitution of the benzoxazole moiety. Bioorg. Med. Chem. Lett. 2010; 20:346–349. [PubMed: 19914065]
18. Zeng Q, Kwok Y, Kerwin SM, Mangold G, Hurley LH. Design of new topoisomerase II inhibitors based upon a quinobenzoxazine self-assembly model. J. Med. Chem. 1998; 41:4273–4278. [PubMed: 9784102]
19. Sampson BA, Misra R, Benson SA. Identification and characterization of a new gene of *Escherichia coli* K-12 involved in outer membrane permeability. Genetics. 1989; 122:491–501. [PubMed: 2547691]
20. Braun M, Silhavy TJ. Imp/OstA is required for cell envelope biogenesis in *Escherichia coli* . Mol. Microbiol. 2002; 45:1289–1302. [PubMed: 12207697]
21. Ravishankar S, Ambady A, Awasthy D, Mudugal NV, Menasinakai S, Jatheendranath S, Guptha S, Sharma S, Balakrishnan G, Nandishaiah R, Ramachandran V, Eyermann CJ, Reck F, Rudrapatna S, Sambandamurthy VK, Sharma UK. Genetic and chemical validation identifies *Mycobacterium tuberculosis* topoisomerase I as an attractive anti-tubercular target. Tuberculosis. 2015; 95:589–598. [PubMed: 26073894]
22. Ahmed W, Menon S, Godbole AA, Karthik PVDNB, Nagaraja V. Conditional silencing of topoisomerase I gene of *Mycobacterium tuberculosis* validates its essentiality for cell survival. FEMS Microbiol. Lett. 2014; 353:116–123. [PubMed: 24593153]
23. Cramer RD, Patterson DE, Bunce JD. Comparative molecular field analysis (CoMFA). 1. Effect of shape on binding of steroids to carrier proteins. J. Am. Chem. Soc. 1988; 110:5959–5967. [PubMed: 22148765]
24. Narula G, Annamalai T, Aedo S, Cheng B, Sorokin E, Wong A, Tse-Dinh Y-C. The strictly conserved Arg-321 residue in the active site of *Escherichia coli* topoisomerase I plays a critical role in DNA rejoining. J. Biol. Chem. 2011; 286:18673–18680. [PubMed: 21478161]
25. Hallett P, Grimshaw AJ, Wigley DB, Maxwell A. Cloning of the DNA gyrase genes under tac promoter control: overproduction of the gyrase A and B proteins. Gene. 1990; 93:139–142. [PubMed: 2172086]
26. Andrews JM. Determination of minimum inhibitory concentrations. J. Antimicrob. Chemother. 2001; 48:5–16. [PubMed: 11420333]
27. Falzari K, Zhu Z, Pan D, Liu H, Hongmanee P, Franzblau SG. In vitro and in vivo activities of macrolide derivatives against *Mycobacterium tuberculosis* . Antimicrob. Agents Chemother. 2005; 49:1447–1454. [PubMed: 15793125]
28. SYBYL-X/QSAR. Molecular Modelling Software. St. Louis, Missouri, 63144, USA: Tripos International, 1699 South Hanley Rd;
29. Masand VH, Mahajan DT, Alafeefy AM, Bukhari SNA, Elsayed NN. Optimization of antiproliferative activity of substituted phenyl 4-(2-oxoimidazolidin-1-yl) benzenesulfonates: QSAR and CoMFA analyses. Eur. J. Pharm. Sci. 2015; 77:230–237. [PubMed: 26066412]
30. Podlogar BL, Poda GI, Demeter DA, Zhang SP, Carson JR, Neilson LA, Reitz AB, Ferguson DM. Synthesis and evaluation of 4-(N,N-diarylamino)piperidines with high selectivity to the delta-opioid receptor: a combined 3D-QSAR and ligand docking study. Drug Des. Discov. 2000; 17:34–50. [PubMed: 10928448]
31. Ståhle L, Wold S. Partial least squares analysis with cross-validation for the two-class problem: A Monte Carlo study. J. Chemom. 1987; 1:185–196.

Highlights

- Fluoroquinophenoxazines were synthesized as bacterial topoisomerase IA inhibitors.
- Some derivatives showed excellent inhibitory activity against topoisomerase IA.
- CoMFA analysis was performed to investigate the 3D-QSAR of this chemical series.
- The constructed CoMFA model produced reasonable and good statistics.

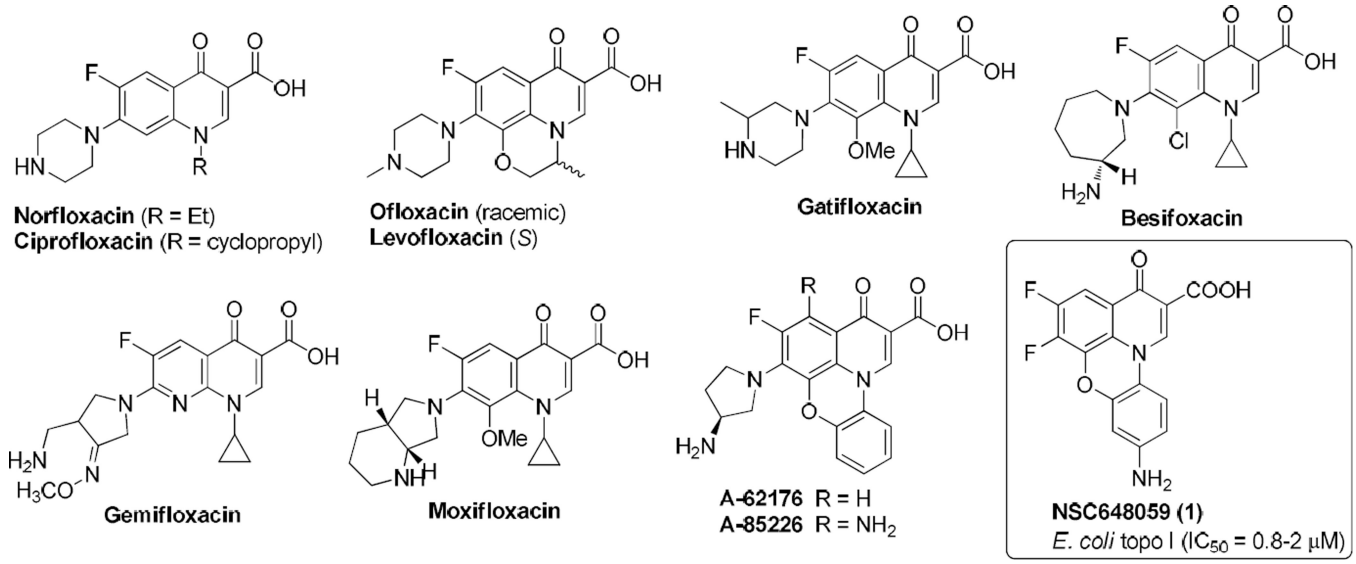

Fig. 1.

Chemical structures of clinical fluoroquinolone antibiotics and fluoroquinophenzoxazine derivatives including our topo I inhibitor **1**.

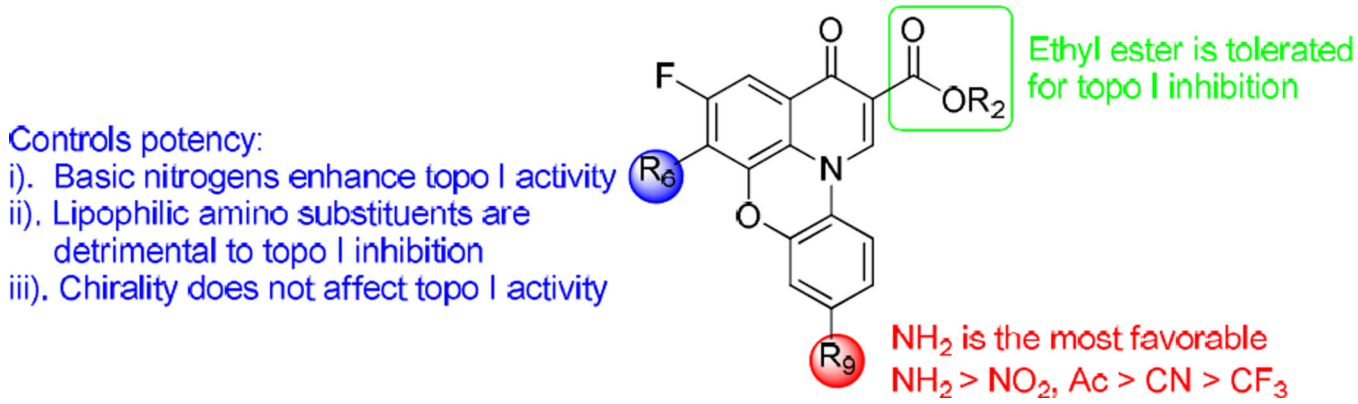

Fig. 2.
SAR toward *E. coli* topoisomerase I inhibition.

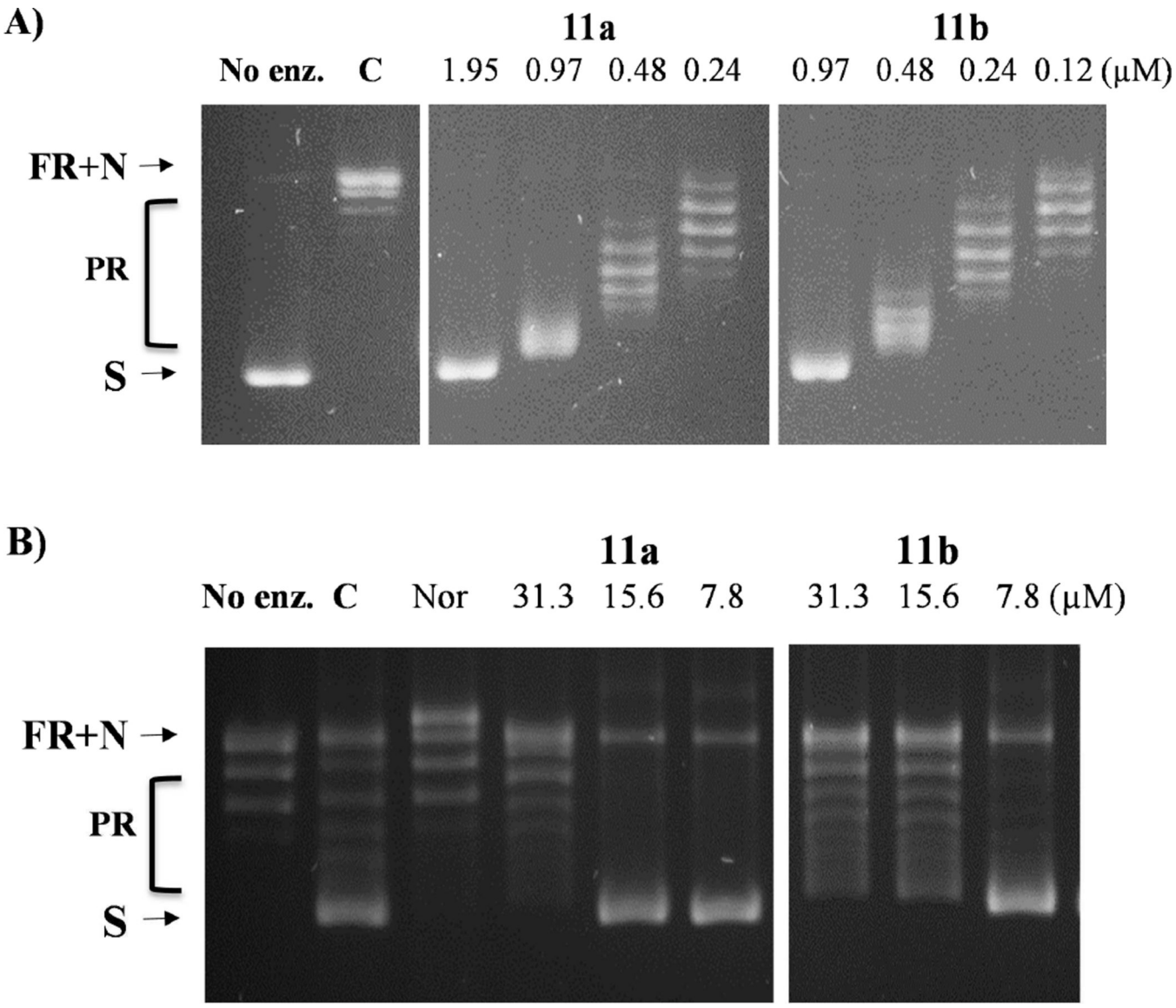

Fig. 3.

Inhibition of *E. coli* topoisomerase relaxation activity by representative **11a** and **11b**. A) *E. coli* topoisomerase I inhibition assays with supercoiled plasmid DNA. B) *E. coli* DNA gyrase inhibition assays with relaxed plasmid DNA. C: DMSO control; Nor: Norfloxacin (125 μM) control; S: Supercoiled plasmid DNA; N: Nicked DNA; FR: Fully relaxed DNA; PR: Partially relaxed DNA.

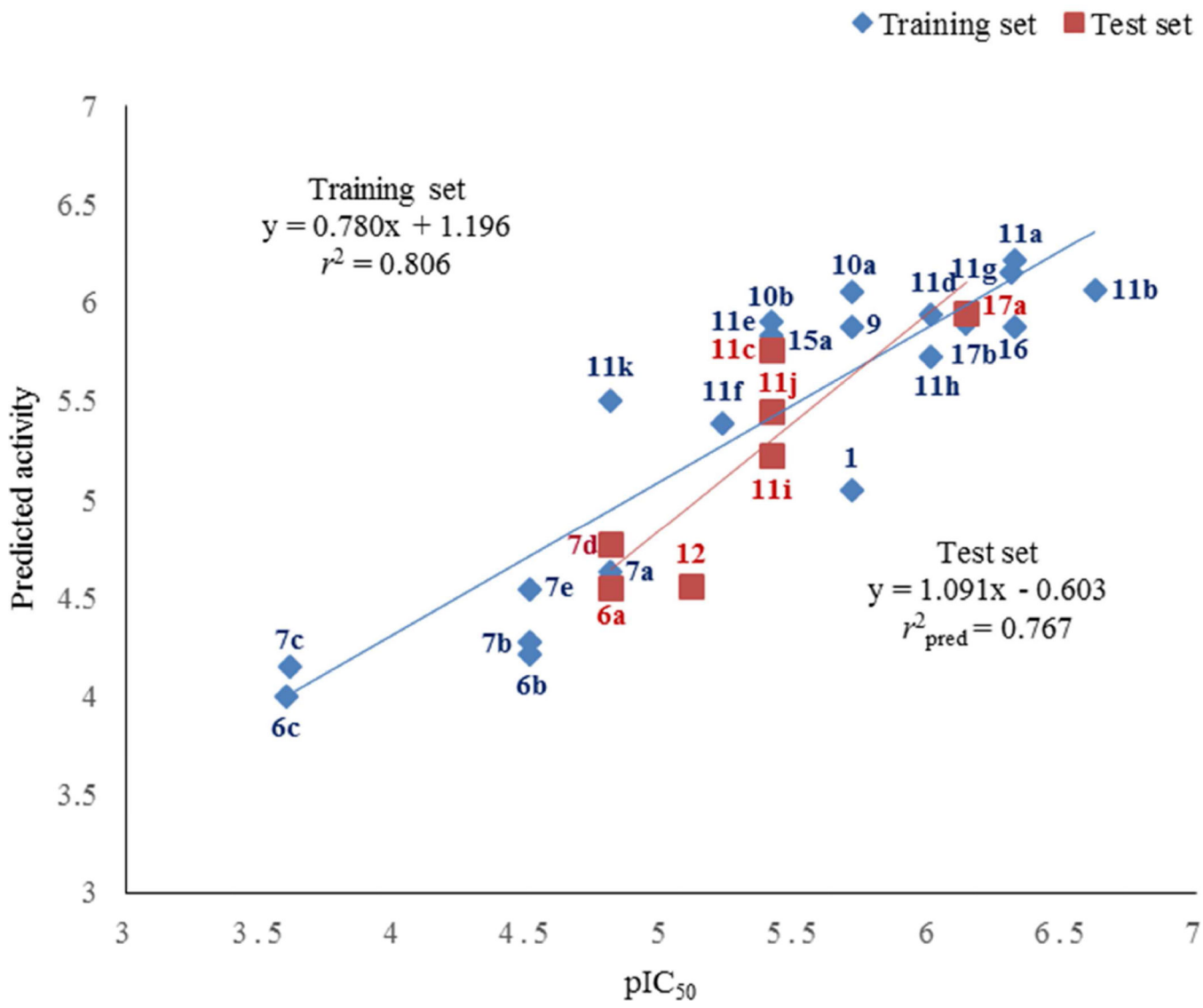

Fig. 4.

The correlation chart of experimental versus predicted values for the training and test set compounds.

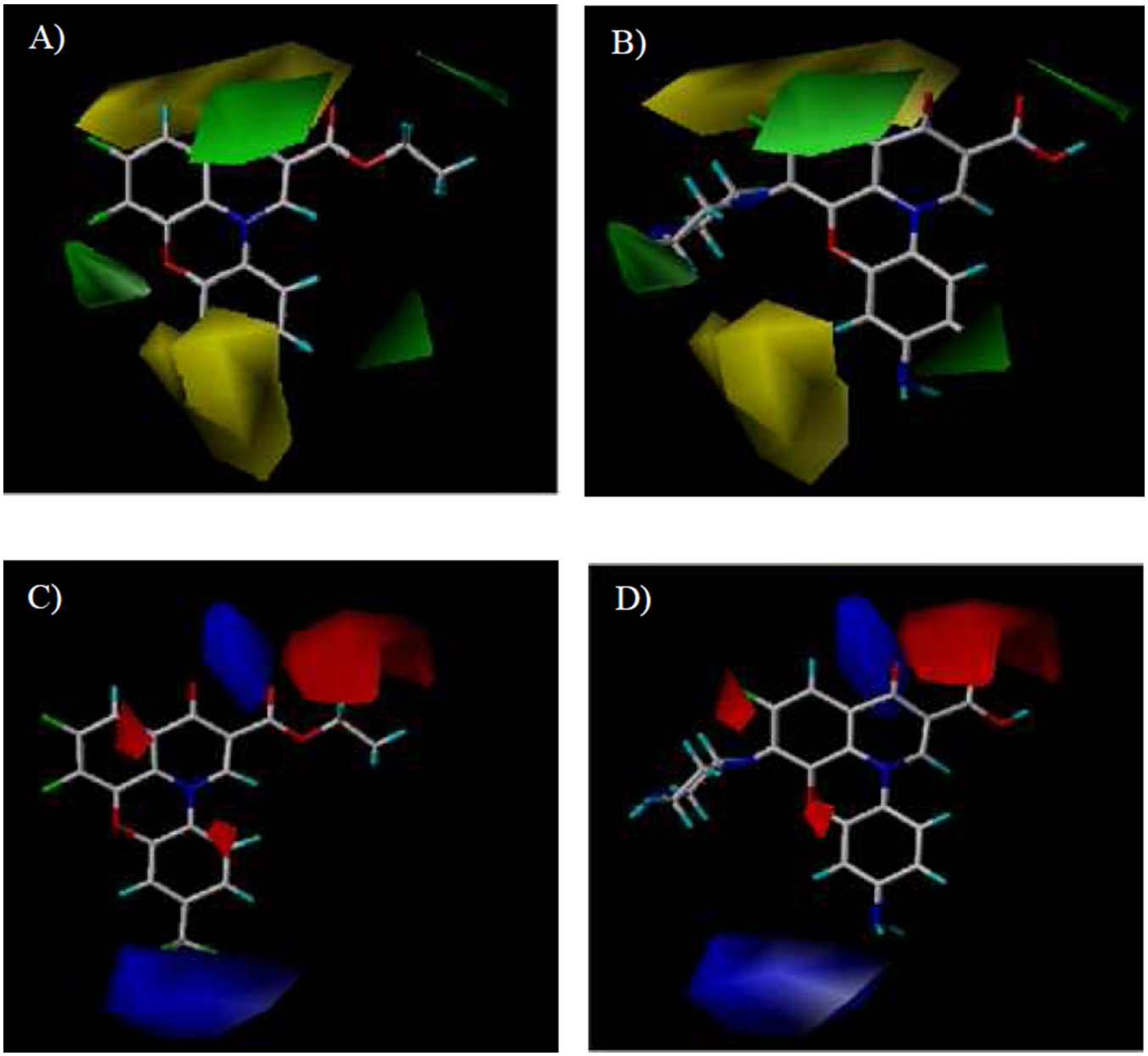

Fig. 5.

Representative CoMFA steric and electrostatic contour maps. A). Steric contour maps with **6c**; B). Steric contour maps with **11b**; C). Electrostatic contour maps with **6c**; and D) Electrostatic contour maps with **11b**.

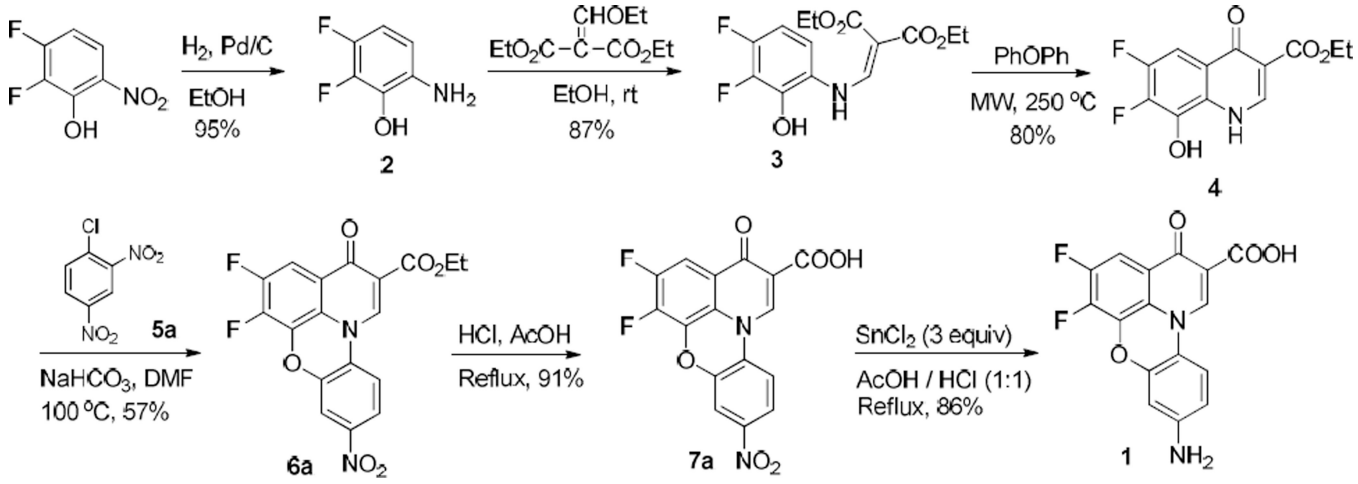

Scheme 1.

Synthesis of 9-amino-5, 6-difluoro-3-oxo-3*H*–pyrido[3,2,1-kl] phenoxazine-2-carboxylic acid (**1**).

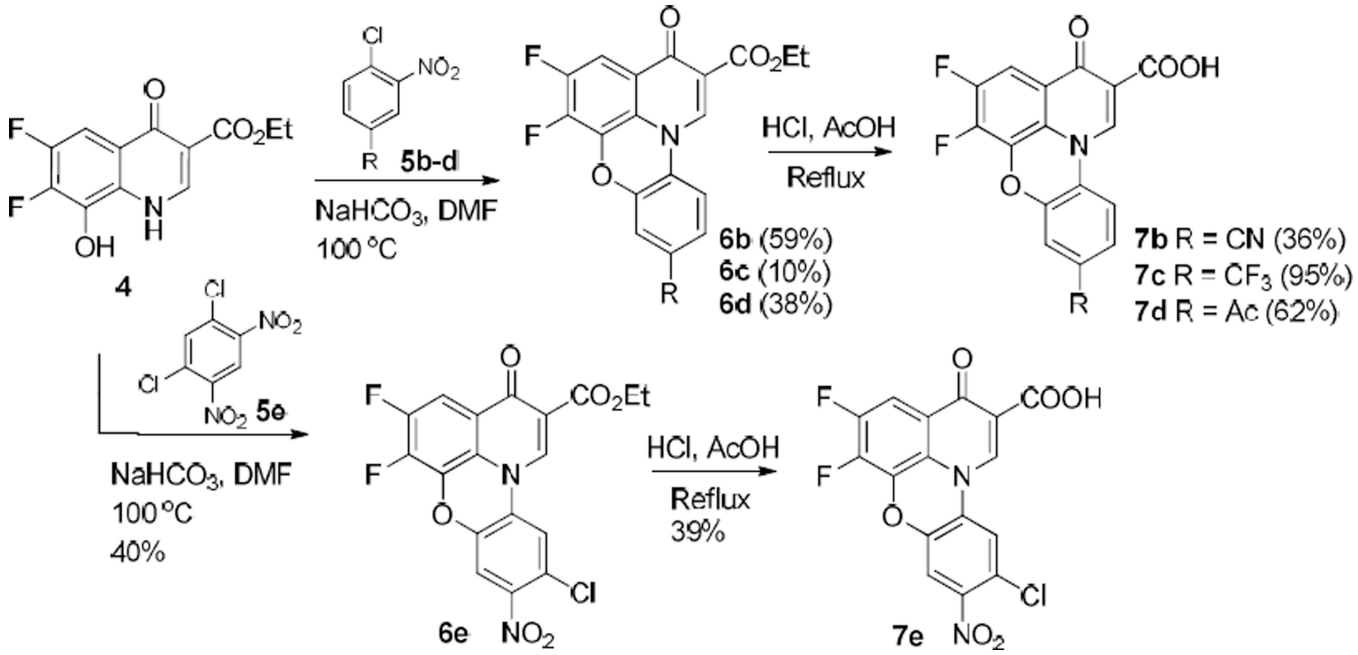

Scheme 2.

Synthesis of fluoroquinophenoxazine derivatives **7b–e**.

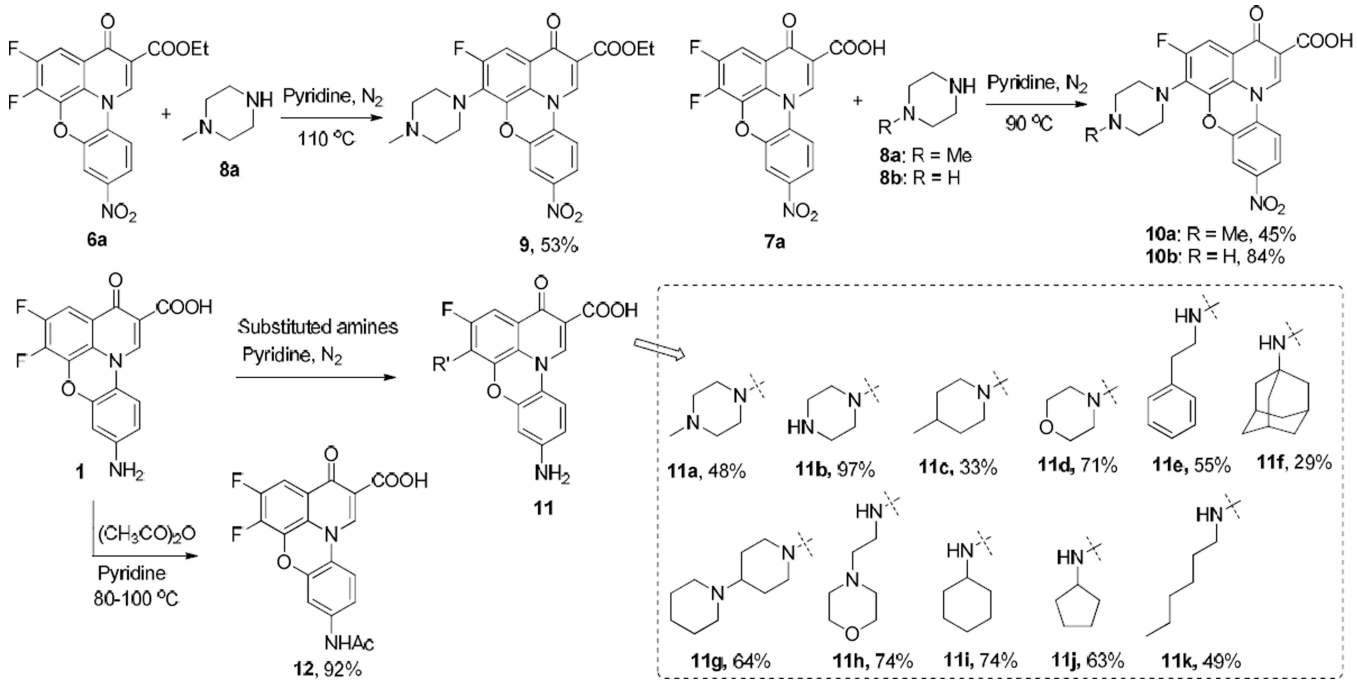

Scheme 3.

Synthesis of diverse amino-substituted fluoroquinophenoxazines **9–11** and acetyl-protected quinophenoxazine **12**.

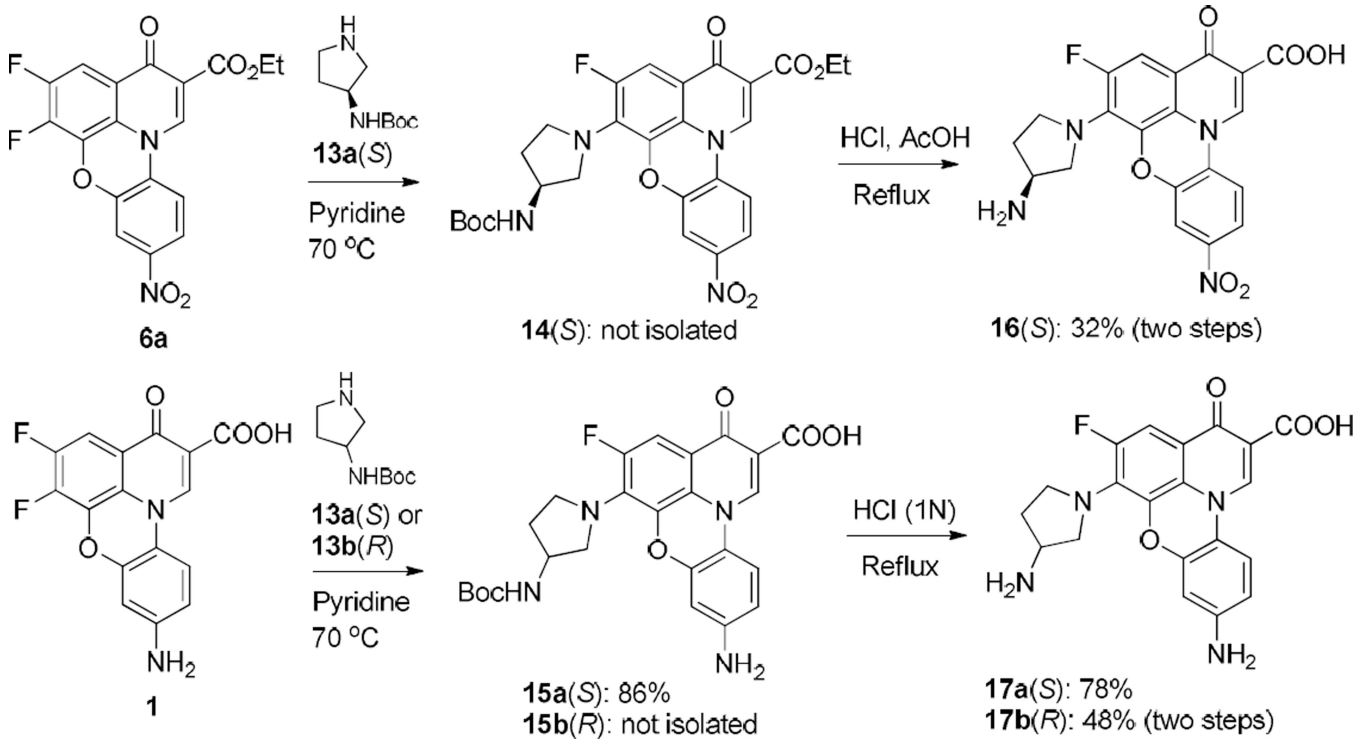

Scheme 4.

Synthesis of fluoroquinophenoxazine chiral amine derivatives **16** and **17**.

Table 1

E. coli topoisomerase I inhibition and whole cell antibacterial activities (μM) of fluoroquinophenoxazine derivatives[a]

	Topoisomerase inhibitory activity (IC_{50}, μM)				Whole cell based antibacterial activity (MIC, μM)					
Compd	***E. coli* topo I (type IA)**	***E. coli* DNA gyrase (type IIA)**	**Human topo I (type IB)**	**Human topo IIα (type IIA)**	***E. coli Imp4213* (BAS3023)**	***E. coli* (MG1655) WT**	***B. subtilis* (ATCC 6633) WT**	***M tuberculosis* ($H_{37}Rv$)**	**Vero cell IC_{50}**	**SI[b]**
1	1.95	>125	31.3	>500	0.78–1.56	>200	6.25	11.2	75.7	6.8
6a	15.6				50	>200	25			
6b	31.25				>200	>200	200			
6c	>125				>200	>200	>200			
7a	15.6				0.78	200	12.5			
7b	31.25				200	>200	>200			
7c	>125				>200	>200	25			
7d	15.6				>200	>200	>200			
7e	31.25	62.5	31.25	125	0.39	50	3.12	29	>127	>4.4
9	1.95				25	>200	50			
10a	1.95	62.5–125	31.25	250–500	1.56	100	0.78	19	95	5.0
10b	3.9				>200	>200	>200			
11a	0.48	15.6–31.25	15.6	3.9–7.8	0.78	6.25	0.78	7.6	29	3.8
11b	0.24	7.8–15.6	7.8	1.95–3.9	0.39	>200	25	29.5	>126	>4.3
11c	3.9				3.12	>200	0.78			
11d	0.97	7.8	15.6	15.6	0.19–0.39	>200	0.19	3.5	24.7	7.1
11e	3.9				50	>200	25–50			
11f	3.9–7.8				3.12	>200	12.5	38.4	30.7	0.8
11g	0.48	15.6	3.9	1.95–3.9	0.39–0.78	>200	1.56	2.5	24.4	9.8
11h	0.97	15.6–31.25	7.8–15.6	3.9–7.8	0.78	>200	1.56	21.6	43.0	2.0
11i	3.9				25	>200	12.5			
11j	3.9				25	>200	12.5			
11k	15.6				>200	>200	>200			
12	7.8				>200	>200	>200			
15a	3.9				12.5	>200	12.5			
16	0.48	3.9	7.8	1.95–3.9	1.56	>200	0.78	>50	>50	

Compd	Topoisomerase inhibitory activity (IC_{50}, μM)				Whole cell based antibacterial activity (MIC, μM)					SI[b]
	E. coli topo I (type IA)	*E. coli* DNA gyrase (type IIA)	Human topo I (type IB)	Human topo IIα (type IIA)	*E. coli Imp4213* (BAS3023)	*E. coli* (MG1655) WT	*B. subtilis* (ATCC 6633) WT	*M tuberculosis* ($H_{37}Rv$)	Vero cell IC_{50}	
17a	0.48–0.97	3.9	3.9	0.97–1.95	1.56	>200	6.25	>63.1	>63.1	
17b	0.48–0.97	3.9	3.9	3.9	6.25	>200	12.5	>63.1	>63.1	

[a] Blank cells indicate Not Determined.

[b] Selectivity index = cytotoxic IC_{50} against Vero cells/MIC against *M. tuberculosis*.

Table 2

Experimental (pIC_{50}) and CoMFA predicted activity (PA) values and residuals for the training and test set compounds[a]

Entry	Compd.	IC_{50} (μM)	pIC_{50}	CoMFA PA[b]	Δ[c]
1	**1**	1.95	5.71	5.05	0.66
2	**6b**	31.25	4.51	4.21	0.30
3	**6c**	250	3.60	4.00	−0.40
4	**7a**	15.6	4.81	4.63	0.18
5	**7b**	31.25	4.51	4.27	0.24
6	**7c**	250	3.61	4.15	−0.54
7	**7e**	31.25	4.51	4.54	−0.03
8	**9**	1.95	5.71	5.88	−0.17
9	**10a**	1.95	5.71	6.05	−0.34
10	**10b**	3.9	5.41	5.90	−0.49
11	**11a**	0.48	6.32	6.21	0.11
12	**11b**	0.24	6.62	6.06	0.56
13	**11d**	0.97	6.01	5.94	0.07
14	**11e**	3.9	5.41	5.83	−0.42
15	**11f**	5.85	5.23	5.39	−0.16
16	**11g**	0.48	6.31	6.15	0.16
17	**11h**	0.97	6.01	5.72	0.29
18	**11k**	15.6	4.81	5.50	−0.69
19	**15a**	3.9	5.41	5.77	−0.36
20	**16**	0.48	6.32	5.88	0.44
21	**17b**	0.73	6.14	5.89	0.25
22	**6a**	15.6	4.81	4.55	0.26
23	**7d**	15.6	4.81	4.77	0.04
24	**11c**	3.9	5.41	5.76	−0.35
25	**11i**	3.9	5.41	5.23	0.18
26	**11j**	3.9	5.41	5.45	−0.04
27	**12**	7.8	5.11	4.56	0.55
28	**17a**	0.73	6.14	5.95	0.19

[a] Entries 1–21 for training set; entries 22–28 for test set.

[b] Predicted activity.

[c] Residual of experimental and predicted activity values.